The evolutionary history of the Central Asian steppe-desert taxon Nitraria (Nitrariaceae) as revealed by integration of fossil pollen morphology and molecular data

Amber Woutersen, Phillip E Jardine, Daniele Silvestro, Raul Giovanni Bogotá-Angel, Hong-Xiang Zhang, Niels Meijer, Johannes Bouchal, Natasha Barbolini, Guillaume Dupont-Nivet, Andreas Koutsodendris, et al.

Botanical Journal of the Linnean Society, 2023, **202**, 195–214. With 8 figures.

The evolutionary history of the Central Asian steppe-desert taxon *Nitraria* (Nitrariaceae) as revealed by integration of fossil pollen morphology and molecular data

AMBER WOUTERSEN[1,*], PHILLIP E. JARDINE[2], DANIELE SILVESTRO[3,4], RAUL GIOVANNI BOGOTÁ-ANGEL[5], HONG-XIANG ZHANG[6], NIELS MEIJER[7], JOHANNES BOUCHAL[8], NATASHA BARBOLINI[9,10], GUILLAUME DUPONT-NIVET[11,12], ANDREAS KOUTSODENDRIS[13], ALEXANDRE ANTONELLI[4,14,15] and CARINA HOORN[1]

[1]*Institute for Biodiversity and Ecosystem Dynamics (IBED), University of Amsterdam, 1098 XH Amsterdam, The Netherlands*
[2]*Institute of Geology and Palaeontology, University of Münster, 48149 Münster, Germany*
[3]*Department of Biology, University of Fribourg, Chemin du Musée 10, Fribourg, Fribourg, Switzerland*
[4]*Gothenburg Global Biodiversity Centre, Department of Biological and Environmental Sciences, University of Gothenburg, Carl Skottsbergs gata 22B, Göteborg, Sweden*
[5]*Facultad del Medio Ambiente y Recursos Naturales, Universidad Distrital Francisco José de Caldas, Carrera 7 No. 40B - 53, Bogotá, Colombia*
[6]*State Key Laboratory of Desert and Oasis Ecology, Xinjiang Institute of Ecology and Geography, Chinese Academy of Sciences, Urumqi, 830011, China*
[7]*Senckenberg Research Institute, 99423 Weimar, Germany*
[8]*Research Group on Aerobiology and Pollen Information, Department of Oto-Rhino-Laryngology, Medical University Vienna, 1090 Vienna, Austria*
[9]*Department of Ecology, Environment and Plant Sciences and Bolin Centre for Climate Research, Stockholm University, SE-106 91 Stockholm, Sweden*
[10]*Department of Biological Sciences, University of Bergen and Bjerknes Centre for Climate Research, 5006 Bergen, Norway*
[11]*Geosciences Rennes UMR-CNRS, Université de Rennes, 35042 Rennes, France*
[12]*Institute of Earth and Environmental Science, University of Potsdam, 14476 Potsdam, Germany*
[13]*Institute of Earth Sciences, Heidelberg University, Heidelberg, 69117 Heidelberg, Germany*
[14]*Department of Plant Sciences, University of Oxford, Oxford, Oxford OX1 3RB, UK*
[15]*Royal Botanic Gardens, Kew, Richmond, Surrey TW9 3AE, UK*

2023Received 15 February 2022; revised 17 July 2022; accepted for publication 11 October 2022

The transition from a greenhouse to an icehouse world at the Eocene-Oligocene Transition (EOT) coincided with a large decrease of pollen from the steppe-adapted genus *Nitraria*. This genus, now common along the Mediterranean coast, Asia and Australia, has a proposed coastal origin and a geographically widespread fossil record. Here we investigated the evolution, taxonomic diversity and morphological disparity of *Nitraria* throughout the Cenozoic by integrating extant taxa and fossil palynological morphotypes into a unified phylogenetic framework based on both DNA sequences and pollen morphological data. We present the oldest fossil pollen grain of *Nitraria*, at least 53 Myr old. This fossil was found in Central Asian deposits, providing new evidence for its origin in this area. We found that the EOT is an evolutionary bottleneck for *Nitraria*, coinciding with retreat of the proto-Paratethys Sea, a major global cooling event and a turnover in Central Asian steppe vegetation. We infer the crown age of modern *Nitraria* spp. to be significantly younger (Miocene) than previously estimated (Palaeocene). The diversity trajectory

*Corresponding author. E-mail: amberwoutersen@gmail.com

of *Nitraria* inferred from extant-only taxa differs markedly from one that also considers extinct taxa. Our study demonstrates it is therefore critical to apply an integrative approach to fully understand the plant evolutionary history of Nitrariaceae.

ADDITIONAL KEYWORDS: desert – Eurasian steppe – light microscopy – phylogeny – SEM – Tibetan Plateau.

INTRODUCTION

During the Eocene-Oligocene Transition (EOT), global temperatures declined driving the climate from greenhouse to icehouse conditions (DeConto & Pollard, 2003; Coxall *et al.*, 2005; Zachos & Kump, 2005). In Central Asia [including Mongolia, northern and western China, and central (geographic) Tibet], this climate change was intertwined with processes such as the retreat of the proto-Paratethys Sea, the India-Asia collision, Tibetan topographic growth and reduction of the monsoons and the hydrological cycle, all resulting in inland aridification (Dupont-Nivet *et al.*, 2007; Dupont-Nivet *et al.*, 2008; Bosboom *et al.*, 2014; Bougeois *et al.*, 2018; Li *et al.*, 2018; Wang *et al.*, 2020). Cenozoic aridification led the Central Asian vegetation into a regime shift at the EOT: the Eocene humid steppe vegetation disappeared almost completely and was replaced by a hyper-arid desert in the Oligocene (Barbolini *et al.*, 2020).

One of the plant genera that was largely impacted by the transition from humid to hyper-arid desert was *Nitraria* L. (Fig. 1). *Nitraria* belongs to Nitrariaceae (Sapindales), which also includes the genera *Peganum* L. and *Tetradiclis* Steven ex M.Bieb. *Peganum* and *Tetradiclis* (four and two accepted species, respectively; WCVP, 2023) occur in arid to semi-arid regions in Africa, the Middle East, central Asia and North America (Abbott *et al.*, 2007; Zhao *et al.*, 2011). *Nitraria* (nine accepted species; WCVP, 2023) is an important proxy for aridity (Su *et al.*, 2016; Yin *et al.*, 2020) and it is also a halophyte (i.e. adapted to saline environments) commonly found in coastal settings. *Nitraria retusa* (Forssk.) Asch., for instance, can be found along the coasts of northern and western Africa and the Middle East, whereas *Nitraria schoberi* L. occurs in the coastal regions of Papua New Guinea and, with *Nitraria billardierei* DC., in southern Australia (Fig. 2a; Woutersen *et al.*, 2018). However, the genus also includes a number of species endemic to Central Asia (*Nitraria sphaerocarpa* Maxim., *Nitraria pamirica* L.I.Vassiljeva, *Nitraria roborowskii* Kom., *Nitraria sibirica* Pall., *N. schoberi* and *Nitraria tangutorum* Bobrov), of which some are part of the steppe-desert vegetation on the Tibetan Plateau, far from any coastal environment and/or influence (Woutersen *et al.*, 2018).

Zhang *et al.* (2015) hypothesized an Early Palaeogene (65 Mya) origin of *Nitraria* based on molecular data and proposed the eastern Tethys (Central Asia; Fig. 2b) as the place of origin [for other taxonomical studies on *Nitraria*, see Pan *et al.* (1999); Temirbayeva & Zhang (2015)]. They explained the present distribution of *Nitraria* in Central Asia as a relic of former marine conditions and proposed that the diversity of *Nitraria* only increased from the Miocene onwards (Zhang *et al.*, 2015). The fossil record, however, shows that *Nitraripollis* Xi Yizhen & Sun Mengrong, 1987 / *Nitrariadites* Zhu & Xi Ping, 1985 (fossil pollen with resemblance to *Nitraria*) flourished both in abundance and diversity during the Palaeogene (Wang *et al.*, 1990a; Hoorn *et al.*, 2012), when the preferred habitat of *Nitraria* (humid steppe vegetation and coastal areas) was abundant (Barbolini *et al.*, 2020). Contrary

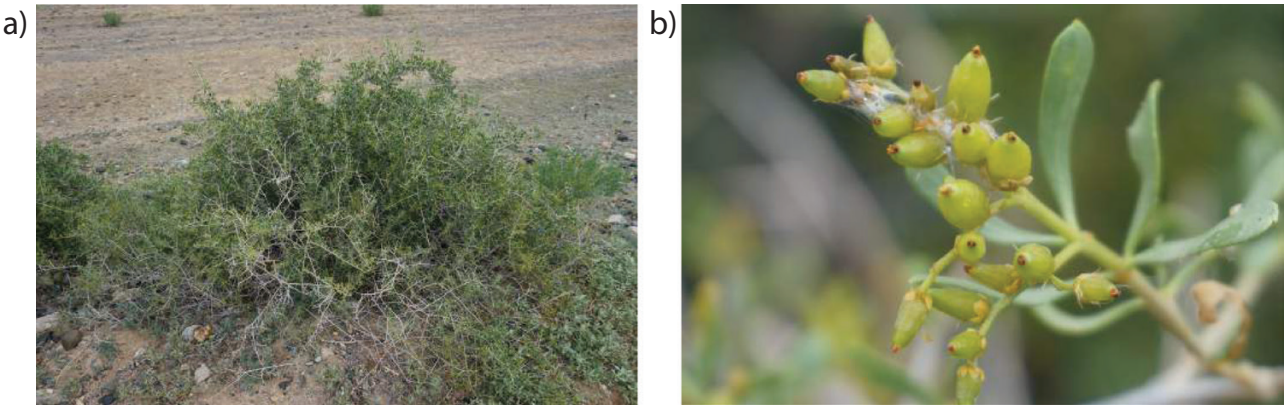

Figure 1. A, Photograph of Nitrariaceae bush. Photo credit: Hong-Xiang Zhang. B, Photograph of *Nitraria* berry. Photo credit: Hong-Xiang Zhang. Both photos were taken on the southern margin of the Junggar Basin.

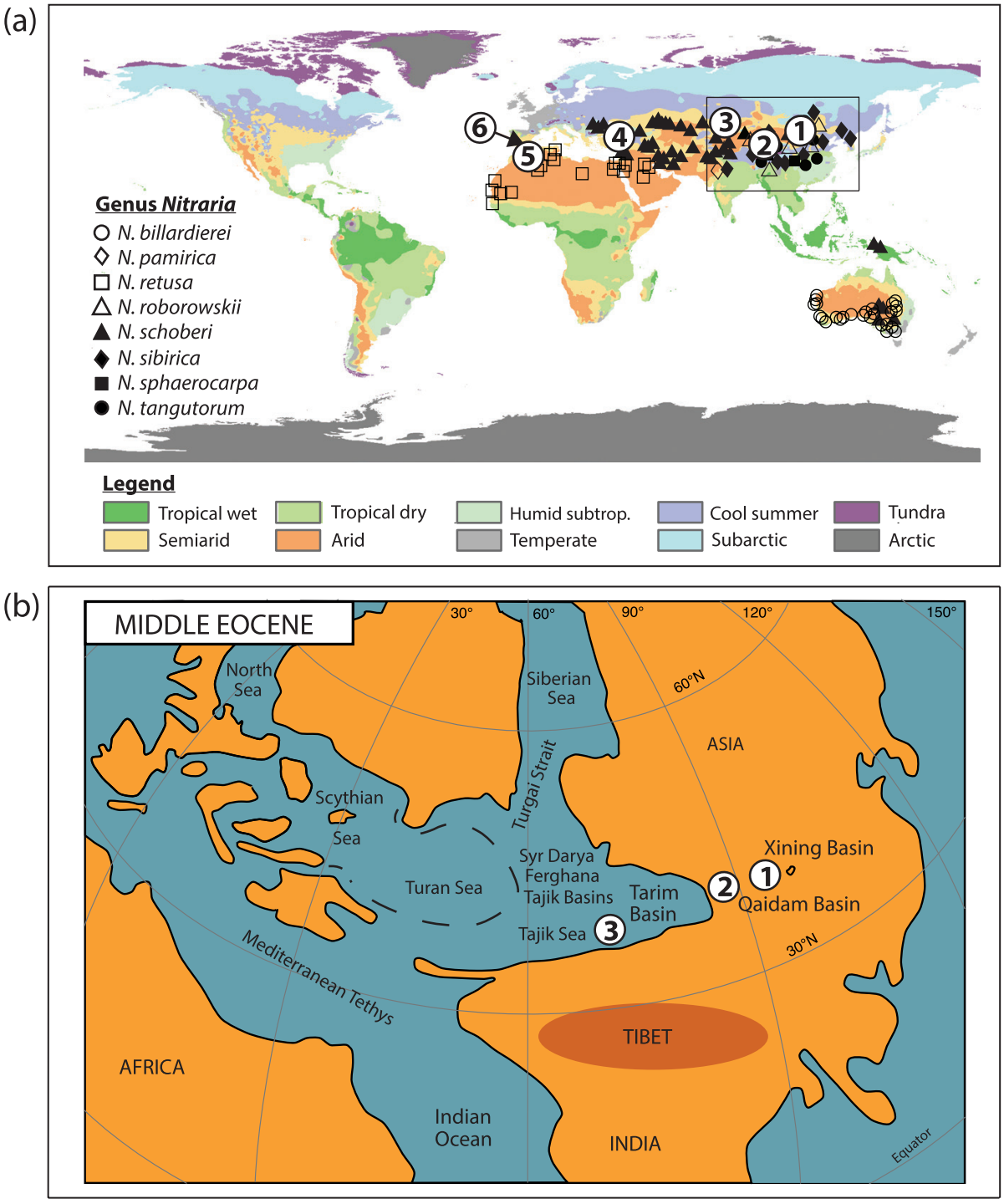

Figure 2. A, Map showing the occurrences of extant *Nitraria* species and the range of fossil occurrences, based on core/section locations. 1, Xining Basin, China (Hoorn *et al.*, 2012); 2, Qaidam Basin, China (Miao *et al.*, 2011, 2013 (Lanzhou), 2016; Koutsodendris *et al.* 2019); 3, Tarim Basin, China (this study); 4, Turkey, Black Sea (Kaya *et al.*, 2007; Ersoy *et al.*, 2014; Bouchal *et al.*, 2016, 2017; Denk *et al.*, 2019); 5, Spain, Algeria (Bessais & Cravatte, 1988; López-Martínez, 1985; de Bruijn *et al.*, 1990; Cavagnetto & Anadón, 1996; Rodríquez-Fernández *et al.*, 1999); 6, South-West Spain (Larrasoaña *et al.*, 2008). Square indicates the range of Figure 1b. B, Map showing the palaeo-reconfiguration of Central Asia, with the proto-Paratethys Sea covering large areas. The Xining (1), Qaidam (2) and Tarim (3) basins and region of uplift on the Tibetan Plateau are indicated, as well as the outline of the future Paratethys Sea (dashed line).

to the model of Zhang *et al.* (2015), *Nitraria* dwindled in the Oligocene, never regaining its Palaeogene level of abundance and species diversity (Miao *et al.*, 2011, 2016). Moreover, at present *Nitraria* forms a minor ecological component of the Tibetan steppe vegetation (Wang *et al.*, 1990b; Hoorn *et al.*, 2012; Han *et al.*, 2016; Koutsodendris *et al.*, 2018).

To better understand the evolutionary history of a clade like *Nitraria*, multiple lines of evidence from living and extinct taxa must be integrated (Ricklefs, 2007; Quental & Marshall, 2010). The modern distribution and species richness of clades is the result of long-term evolutionary and biogeographic processes and inferring those processes solely from living species can be deceiving. Fossil data are therefore used in, for example, geographical range analyses (e.g. Nauheimer *et al.*, 2012), to calibrate phylogenetic trees (e.g. Barba-Montoya *et al.*, 2018; Crisp *et al.*, 2019) and in the construction of phylogenetic trees in so-called total evidence analyses (e.g. Manos *et al.*, 2007; Yu *et al.*, 2016). Other studies have also shown the relevance of integrating fossil data in evolutionary analyses, including the estimation of diversification rates (Mitchell *et al.*, 2018; Silvestro *et al.*, 2018; Warnock *et al.*, 2020) and trait evolution (Slater, 2015; Hunt & Slater, 2016; Silvestro *et al.*, 2019). The complex evolutionary history of *Nitraria* (Fig. 1) could potentially be solved by applying such an integrative approach.

In 2018, Woutersen *et al.* (2018) showed that for modern *Nitraria*, combining pollen morphology and phylogenetic data proved a successful method when reconstructing the evolutionary history of species. *Nitraria* pollen morphology holds a clear phylogenetic structure and extant species can be separated based on their measured pollen morphological characters. This implied that pollen could be linked to major lineages in the phylogenetic tree (Woutersen *et al.*, 2018). Applying this approach to the rich fossil palynological record of *Nitraria* should help in solving the differences between molecular records (suggesting a Palaeocene origin and a recent Miocene diversification; Zhang *et al.*, 2015) and palynological records (suggesting high diversity in the Palaeocene and Eocene; Wang *et al.*, 1990a; Hoorn *et al.*, 2012; Han *et al.*, 2016; Barbolini *et al.*, 2020). Furthermore, it enables us to follow the evolutionary dynamics of *Nitraria* during the rapid climate and geological changes at the EOT.

In this study, we trace the evolutionary history of *Nitraria* by combining pollen morphological and molecular data from extant taxa and the fossil palynological record. We document the morphology of extant and fossil *Nitraria* pollen based on light microscopy (LM) and scanning electron microscopy (SEM), and combine these morphological data with a molecular phylogenetic tree in a total evidence phylogenetic tree (Ronquist *et al.*, 2012; Heath *et al.*, 2014). We estimate taxonomic diversity through time and integrate the pollen morphological data and total evidence phylogeny to generate a phylomorphospace and calculate morphological disparity. Taken together, our data illustrate the evolutionary changes of *Nitraria* throughout periods of major climate and landscape changes.

MATERIAL AND METHODS

Palynological records of northern China and the northern Tibetan Plateau

We used well-dated and high-resolution Palaeogene sections that comprise both terrestrial and coastal deposits in Central Asia. We combined the *Nitraripollis*/*Nitrariadites* occurrences in Palaeogene records from the Xining Basin [Shuiwan, Tiefo and Sanhe sections, for age models see Dai *et al.* (2006); Dupont-Nivet *et al.* (2007); Abels *et al.* (2011); Bosboom *et al.* (2014); Meijer (2021)] and the Tarim Basin [Mine Section, for age model see Kaya *et al.* (2019)], with Neogene and Quaternary records. The latter consisted of Miocene, Pliocene and Pleistocene records from the SG-1 and SG-1b core from the Qaidam Basin [Fig. 2; for age models see Zhang *et al.* (2012, 2014); Herb *et al.* (2015)]. Palynological data on the Shuiwan, Tiefo, SG-1 and SG-1b sections were previously published by Hoorn *et al.* (2012), Bosboom *et al.* (2014) and Koutsodendris *et al.* (2018, 2019), respectively, and for these sections we report additional data here. Palynological data on the Mine and Sanhe sections are first published in this study. At present, the Xining, Qaidam and Tarim basins all belong to the desert/steppe-desert ecoregion (Abels *et al.*, 2011; Cai *et al.*, 2012; Hoorn *et al.*, 2012; Bosboom *et al.*, 2014; Han *et al.*, 2016; Wang *et al.*, 2021). For more information about the geological and climatological settings, see Supporting Information, Data S1.

Processing method

Palaeogene samples from the Shuiwan, Tiefo and Sanhe sections in the Xining Basin were previously processed at Vrije Universiteit Amsterdam, the Netherlands (Hoorn *et al.*, 2012) and at Palynological Laboratory Services (PLS) PalyLab, UK (Sanhe). Preparation of the samples from the Mine Section (Tarim Basin) followed standardized techniques described in Houben *et al.* (2011). Miocene and Pleistocene samples from the SG-1 and SG-1b cores from the Qaidam Basin were processed at Heidelberg University following standard palynological techniques (Koutsodendris *et al.*, 2018, 2019). Pliocene samples from the SG-1b core were processed at the University of Amsterdam.

Samples were treated with hydrochloric acid and sieved over a 212 µm mesh sieve. Samples were then soaked in sodium pyrophosphate ($Na_4P_2O_7{\cdot}10H_2O$) in a 20% solution with H_2O, followed by acetolysis. Finally, density separation, to separate the inorganic fraction, was performed with bromoform (2.0 g/cm^3)

LM AND SEM MICROPHOTOGRAPHY

Microphotographs were taken of selected specimens with a Zeiss Nomarski differential interference contrast (DIC) microscope (Bercovici *et al.*, 2009). While taking the photographs, we recorded the varying z-axes and images were later combined through manual z-stacking in Adobe Photoshop. This stacking technique combines different layers to provide a sense of depth to the images, with a result comparable to three-dimensional photography. SEM images of pollen grains (different from those photographed with LM) were made at the Institute of Ecology and Geography, China Academy of Sciences, Urumqi, China, and at the Department of Paleontology, University of Vienna, Vienna, Austria. After the standard palynological processing described above, pollen grains were deposited on stubs with a carbon adhesive disc using the single-grain analysis method (Zetter, 1989; Halbritter *et al.*, 2018), and coated with a mixture composed of Gold-Platinum (Au-Pt). The specimens were scanned with a Zeiss EVO SEM (kV ranging from 5 to 15) at Xinjiang University, and with a JEOL JSM·6400 SEM and Zeiss DSM 960 SEM at the University of Vienna. Similar microphotographs are available for the extant taxa in Woutersen *et al.* (2018).

POLLEN MORPHOLOGY

Fossil *Nitraria* pollen types (*Nitrariadites* or *Nitraripollis*) are tricolporate and have a characteristic thick, three-layered, striately patterned exine, with pores that are described as 'cat's eyes' (Zunghao *et al.*, 1985; Xi & Sun, 1987; Hoorn *et al.*, 2012). A large number of fossil taxa have been previously described (mostly in Chinese; Supporting Information, Table S1), and many synonyms for fossil *Nitraria* spp. occur in the literature (Supporting Information, Table S1). Other fossil pollen that resemble *Nitraria* are *Meliaceoidites* Wang, 1980, *Qinghaipollis* Zhu, 1985 and *Pokrovskaja* Boltsova *et al.*, 1979 (Duan *et al.*, 2007; Dupont-Nivet *et al.*, 2009; Miao *et al.*, 2013). Much of the available literature is difficult to retrieve since papers are not available from European university and journal databases (Agababian & Tumanian, 1972; Xi & Sun, 1987; Xi & Zhang, 1991) or it is in Chinese (Xi & Sun, 1987; Xi & Zhang, 1991; Abdusalih & Xiaoling, 2003) and does not reach a broad readership. To avoid adding junior synonyms, we chose to use morphospecies. Although there often are discrepancies between morphospecies and biological species, in the case of *Nitraria*, the morphospecies represents a highly distinctive set of pollen which can be tracked through time (Woutersen *et al.*, 2018).

We distinguished morphospecies based on LM photographs and a matrix comprising 14 morphological, discrete, multistate characters, including information about equatorial and polar shape, number, position and type of apertures, size of pores, and exine thickness, structure and sculpture [following Woutersen *et al.* (2018)]. Characters were scored for both the extant and fossil individual specimens (measurements and observations mainly obtained via LM using a Leitz microscope at 1000 × magnification; Supporting Data S3). We checked for consistent differences in variability within morphological characters between the fossil types and extant species. There were a few characters for which the extant species were more or less variable than the fossil types, but there were no clear and consistent differences across all taxa (see Supporting Information, Fig. 1). In total 49 grains were measured for the Pleistocene, 57 for the Pliocene, 40 for the Miocene and 165 for the Eocene, and 20 specimens were measured for each of the extant taxa (Woutersen *et al.*, 2018). Throughout the Cenozoic, we identified a total of 32 different fossil *Nitraria* morphospecies. For detailed descriptions of all types and LM and SEM photographs, see the Supporting Information (Data S2; Figs S2, S3) and Figures 3 and 4. An overview of the palynological diversity of extant *Nitraria* is available in previous publications (Perveen & Qaiser, 2006; Woutersen *et al.*, 2018).

PHYLOGENETIC ANALYSES

We inferred the phylogeny of extinct and extant *Nitraria* spp. by combining the molecular data of extant taxa from Zhang *et al.* (2015), which included six nuclear and plastid markers, with the pollen morphological character matrix. To our knowledge, this is the first time such an analysis has been done using pollen morphological data. This extends the number of usable fossils that we can include in total evidence analyses (next to, e.g. leaf fossils), especially since pollen is often abundant. The final 'total evidence' dataset included 46 lineages, of which 14 were extant species (including the sister group *Peganum* and outgroups). All species included morphological data, but molecular data were only available for the extant taxa. The alignments and all input files for phylogenetic analyses are available in Supporting Information, Data S3 and S4.

We performed a Bayesian phylogenetic analyses using BEAST v.2.6.3 (Bouckaert *et al.*, 2014) with a fossilized birth-death prior on the node ages (Heath *et al.*, 2014) and a gamma prior on the root age with 95% credible

Figure 3. LM micrographs of fossil *Nitraria* pollen. The sample reference code and England Finder reference follow the (morpho)species name, as follows: a 1-2. *Nitraripollis*/*Nitrariadites* sp., type 16 (MS-BS39; P50/Q50-4); b 1-2. *Nitraripollis*/*Nitrariadites* sp., type 15 (MS-BS39; P48-3); c 1-2. *Nitraripollis*/*Nitrariadites* sp., type 6 (MS-BS39; P49/Q49-4); d 1-2. *Nitraripollis*/*Nitrariadites* sp., type 17 (MS-BS39; M47/N47-4); e 1-3. *Nitraripollis*/*Nitrariadites* sp., type 12 (Temple sectie 2009-1; F61-3); f 1-2. *Nitraripollis*/*Nitrariadites* sp., type 5 (PSW02; G35/G36-4/3). Reproduced from Hoorn *et al.*, 2012; g 1-2. *Nitraripollis*/*Nitrariadites* sp., type 11 (Temple sectie 2009-1; K43-3); h 1-2. *Nitraripollis*/*Nitrariadites* sp., type 2 (PFT02-08; Q39-1); i 1-2. *Nitraripollis*/*Nitrariadites* sp., type 5 (PSW27b; S30/S31-4/3). Reproduced from Hoorn *et al.*, 2012; j 1-2.

Nitraripollis/*Nitrariadites* sp., type 5 (PSW32; J58-2/4). Polar view, reproduced from Hoorn *et al.*, 2012; k 1-2. *Nitraripollis*/*Nitrariadites* sp., type 18 (PSW08-08a; Q43-3); l 1-2. *Nitraripollis*/*Nitrariadites* sp., type 14 (PSW08-08a; Q38/Q39-2); m 1-2. *Nitraripollis*/*Nitrariadites* sp., type 10 (Temple sectie 2009-1; E53/E54/F53/F54); n 1-2. *Nitraripollis*/*Nitrariadites* sp., type 9 (PSW26-08; H36-3); o 1-2. *Nitraripollis*/*Nitrariadites* sp., type 3 (PSW02-08; O32-2). Reproduced from Hoorn *et al.*, 2012; p 1-2. *Nitraripollis*/*Nitrariadites* sp., type 7 (PSW26-08; J33-1). Reproduced from Hoorn *et al.*, 2012; q 1-2. *Nitraripollis*/*Nitrariadites* sp., type 13 (PFT02-08; T37-1); r 1-2. *Nitraripollis*/*Nitrariadites* sp., type 19 (Temple sectie 2009-1; N53); s 1-3. *Nitraripollis*/*Nitrariadites* sp., type 1 (P385; J33-4) Reproduced from Hoorn *et al.*, 2012; t 1-2. *Nitraripollis*/*Nitrariadites* sp., type 8 (PSW27b; P33-4/3). Reproduced from Hoorn *et al.*, 2012; u 1-2. *Nitraripollis*/*Nitrariadites* sp., type 4 (PSW27b; S49-3). Reproduced from Hoorn *et al.*, 2012.

interval spanning from the Mid-Eocene, when the oldest *Nitraria* fossils were found, to the beginning of the Cretaceous (shape = 1.5, scale = 21, offset = 46.6). We used a relaxed clock model with uncorrelated log-normal rate heterogeneity and a GTR+gamma substitution model for molecular data partitioned between nuclear (ITS) and plastid markers (*psbA-trnH*, *psbBH*, *rbcL*, *rps16*, *rps16-trnK*, *trnL-F*). For the morphological data we used a standard Mk (where the 'M' stands for 'Markov' and 'k' refers to the number of states observed; Lewis, 2001) model. For tip calibration, the age of fossil tips was set to the age of the oldest known occurrence of each morphospecies. We used an exponential prior on diversification rate and a uniform prior [0,1] on the turnover rate. We constrained the genera *Nitraria* and *Peganum* to be monophyletic and sister to each other. As we had point estimates of the fossil occurrence ages, we set the tip dates to fixed values. We ran two independent analyses for 100 million Markov chain Monte Carlo iterations with sampling frequency set at 50 000 and combined the posterior sampled trees after excluding the burn-in. We then plotted the number of lineages in Nitrariaceae (*Nitraria*, *Peganum*) through time after removing outgroup lineages (*Tribulus* L., *Zygophyllum* L.) and extending the temporal range of extinct species in the trees based on the youngest known fossil occurrences. The lineages-through-time (LTTs) were computed and summarized as a consensus tree across a sample of 3800 posterior trees. We preferred this type of visualization of lineage accumulation, instead of a formal estimation of speciation and extinction rates, given the recent findings of Louca & Pennell (2020) which indicate identifiability issues in these model estimates and the expected limited statistical power due to the relatively small size of the tree.

Phylomorphospace construction and quantification of morphological disparity

We produced a phylomorphospace (Sidlauskas, 2008; Lloyd, 2018; Woutersen *et al.*, 2018) by combining the pollen morphological character matrix and the total evidence phylogeny in an ordination framework. Specifically, we reconstructed the character states for the nodes of the phylogeny using maximum likelihood estimation (Lloyd, 2018) and then ordinated both the tips and the nodes of the phylogenetic tree using principal coordinates analysis (PCO) of a maximum observable rescaled distance (MORD) distance matrix (Lloyd, 2016, 2018). This corresponds to the 'pre-ordination ancestral character state estimation' of Lloyd (2018: 88). The MORD distances were arcsine square root transformed prior to ordination (Lloyd, 2016). The PCO was carried out with Cailliez correction to ensure that only non-negative eigenvalues were produced (Cailliez, 1983). Missing data were coded as 'NA', and were ignored in the pairwise distance calculations. Both the phylogenetic tree and the taxa were then plotted in the same morphospace (Lloyd, 2018). We also produced a chronophylomorphospace (Sakamoto & Ruta, 2012) by plotting the first two PCO axis scores against a third time axis, using the estimated tip and node ages to plot the taxa and the phylogenetic tree.

Ordinations of discrete character data often suffer from spreading the variance in the data over many axes, rather than concentrating it on the first few (Lloyd, 2016, 2018). We therefore explored two other options for phylomorphospace construction. First, we carried out post-ordination ancestral state estimation (*sensu* Lloyd, 2018: 87), by ordinating just the tips of the phylogenetic tree and estimating ancestral states for the nodes using the ordination axis scores as new continuous characters. The axis scores for the tips and nodes were then used to plot the phylogeny in ordination space, with higher variance concentrated on the first few PCO axes relative to the pre-ordination ancestral state estimation phylomorphospace (see Results, Fig. 6a; Supporting Information, Fig. S4). Second, we repeated the PCO-based analyses using non-metric multidimensional scaling (NMDS), which reached an acceptable stress of 0.15 with a three-axis ordination (Supporting Information, Fig. S5).

Disparity through time was calculated using the time slicing method of Guillerme & Cooper (2018). Rather than considering sampled taxa in discrete time bins, this approach uses a time-calibrated phylogeny to estimate lineage presence through time (that is, using the branches of the phylogeny), allowing disparity to

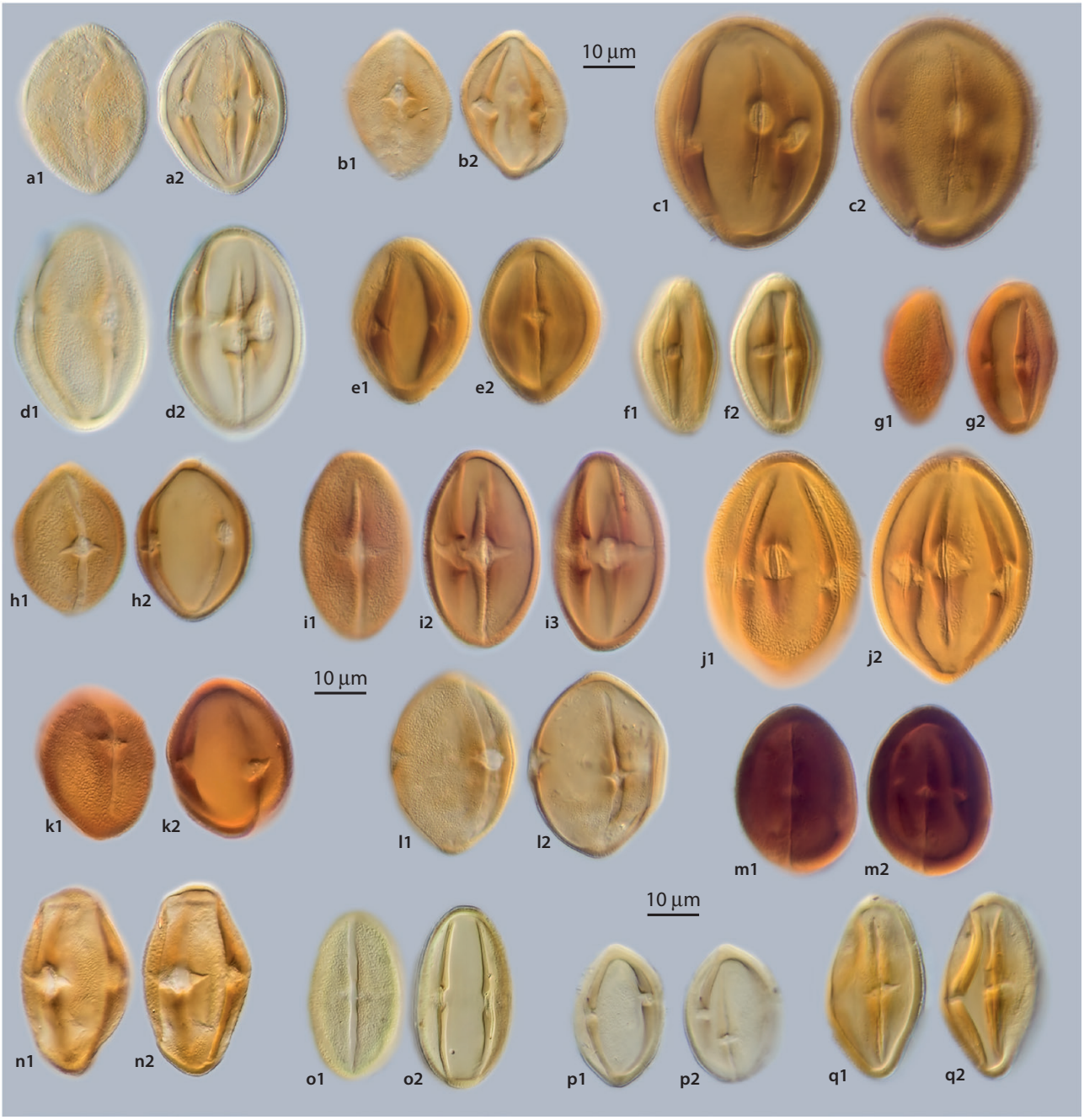

Figure 4. LM micrographs of fossil *Nitraria* pollen. The sample reference code and England Finder reference follow the (morpho)species name, as follows: a 1-2. *Nitraripollis*/*Nitrariadites* sp., type 22 (SG-1b 699; K57) Miocene; b 1-2. *Nitraripollis*/*Nitrariadites* sp., type 20 (SG-1b 715; V52-3) Miocene; c 1-2. *Nitraripollis*/*Nitrariadites* sp., type 21 (SG-1b 715; K41-2) Miocene; d 1-2. *Nitraripollis*/*Nitrariadites* sp., type 24 (SG-1b 599; F28-4) Miocene; e 1-2. *Nitraripollis*/*Nitrariadites* sp., type 25 (SG-1b 671 m; U56/V56) Miocene; f 1-2. *Nitraripollis*/*Nitrariadites* sp., type 23 (SG-1b 599; G49-4) Miocene; g 1-2. *Nitraripollis*/*Nitrariadites* sp., type 23 (SG-1b 325 m; G61-2) Pliocene; h 1-2. *Nitraripollis*/*Nitrariadites* sp., type 20 (SG-1b 220 m; V45-1) Pliocene; i 1-3. *Nitraripollis*/*Nitrariadites* sp., type 24 (SG-1b 145 m; G51-1) Pliocene; j 1-2. *Nitraripollis*/*Nitrariadites* sp., type 27 (SG-1b 310 m; S43-4) Pliocene; k 1-2. *Nitraripollis*/*Nitrariadites* sp., type 28 (SG-1b 310 m; Q51) Pliocene; l 1-2. *Nitraripollis*/*Nitrariadites* sp., type 26 (SG-1b 355 m; G48-2) Pliocene; m 1-2. *Nitraripollis*/*Nitrariadites* sp., type 30 (SG-1b 160.03 m; U56-1) Pliocene; n 1-2. *Nitraripollis*/*Nitrariadites* sp., type 29 (SG-1b 310 m; S57/T57) Pliocene; o 1-2. *Nitraripollis*/*Nitrariadites* sp., type 24 (SG1 202.92 m; S52/S53-4) Pleistocene; p 1-2. *Nitraripollis*/*Nitrariadites* sp., type 31 (SG1 454.44 m; O59-1) Pleistocene; q 1-2. *Nitraripollis*/*Nitrariadites* sp., type 32 (SG1 454.44 m; R52) Pleistocene.

be calculated at equidistant time slices. We measured disparity by calculating the sums of the variances of the ordination axis scores at intervals of 2 Myr. When branches of a phylogenetic tree are used for calculating disparity, it is necessary to use the ordination scores of either the ancestral node or the descendent node/tip, which are selected according to a pre-determined model of character evolution (Guillerme & Cooper, 2018). We used the 'proximity' model (Guillerme & Cooper, 2018), which selects either the ancestor or the descendent according to whether the time slice occurs in the first or second half of the branch, respectively. We calculated disparity across a sample of 1600 posterior trees and then computed the median, 2.5%, 25%, 75% and 97.5% percentiles for each time slice to give a disparity estimate and associated 95% and 50% confidence intervals.

Morphospace and disparity analyses were performed on *Nitraria* and *Nitraripollis/Nitrariadites* types only, that is, excluding *Peganum*, *Tribulus* and *Zygophyllum*. We carried out the morphological analyses in R v.4.0.4 (R Core Team, 2021) using the packages ape v.5.4-1 (Paradis & Schliep, 2019), Claddis v.0.6.3 (Lloyd, 2016), dispRity v.1.5.0 (Guillerme, 2018), gtools v.3.8.2 (Warnes *et al.*, 2020), plot3D v.1.3 (Soetaert, 2019), vegan v.2.5-7 (Oksanen *et al.*, 2020) and viridis v.0.6.1 (Garnier *et al.*, 2021).

RESULTS

The first appearance of fossil *Nitraria* pollen in our records

The oldest *Nitraria* fossil (*Nitraripollis*/*Nitrariadites*; Fig. 5) in our records was found in the Xining Basin and, based on magnetostratigraphy, is dated as Early Eocene (>53 Myr, Meijer *et al.*, 2022). This date is in general agreement with previous findings of fossils assigned a Palaeogene age by Xi & Sun (1987). The oldest documented *Nitraria* pollen type is elliptic and has one slightly pointed and one rounded polar area (Fig. 5). It is more prolate in shape compared to pollen of extant taxa but shares the striate pattern on the outer pollen wall. The pattern is tightly packed, without any perforations of the pollen wall, comparable to the extant *N. sphaerocarpa*. A more detailed description of the oldest documented type can be found in Supporting Information, Data S2. The fossil *Nitraria* grains displayed some of the characteristic morphological variability previously observed in the extant species, such as a perforated vs. non- or poorly-perforated exine (Woutersen *et al.*, 2018). These characteristics can thus be traced throughout the fossil record and stem back to the Palaeogene, directly linking the extant *Nitraria* spp. to the oldest fossils.

Total evidence phylogenetic analysis and lineages through time (LTT)

The total evidence phylogenetic analysis included 32 fossil (extinct) morphospecies, nine extant *Nitraria* spp., three lineages of the sister genus *Peganum* and the outgroup with *Zygophyllum xanthoxylum* (Bunge) Maxim. and *Tribulus terrestris* L. (Fig. 6). Although the relatively low number of morphological traits available for fossil taxa resulted in limited support for fossil nodes in the tree (an expected pattern in total evidence analyses; Ronquist *et al.*, 2012), phylogenetic relationships among extant taxa received high posterior support (Fig. 6), including 0.99 posterior probability supporting the clade including all *Nitraria* and *Nitraripollis* lineages as one clade. LTT plots based on extinct and extant species show that *Nitraria* reached its highest diversity in the Eocene

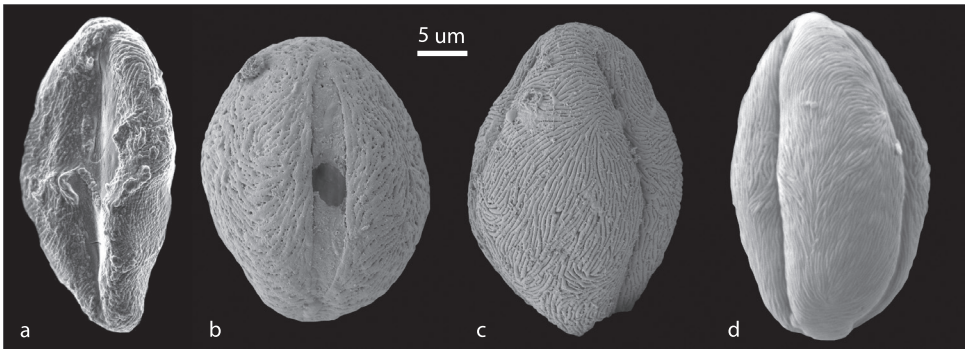

Figure 5. SEM micrographs of *Nitraria* pollen. A, *Nitraripollis*/*Nitrariadites* sp. Age ≤53 Mya (17SH-NB-(-3.5)). Tight striae without perforations on the exine surface. B, *Nitraripollis*/*Nitriadites* sp. Age 36,37 Mya (3_37XJ_P1). Wide striae with perforations on the exine surface. C, *Nitraripollis*/*Nitriadites* sp. Age 36,37 Mya (3_37XJ_P1). Striae on the exine surface. D, *Nitraria sphaerocarpa*. Tight striae on the exine surface. Reproduced from Woutersen *et al.*, 2018. For more detailed photos of B-D see Supplementary Information, Fig. 3 (photo C2/C3) and 4 (photo E2 and B2).

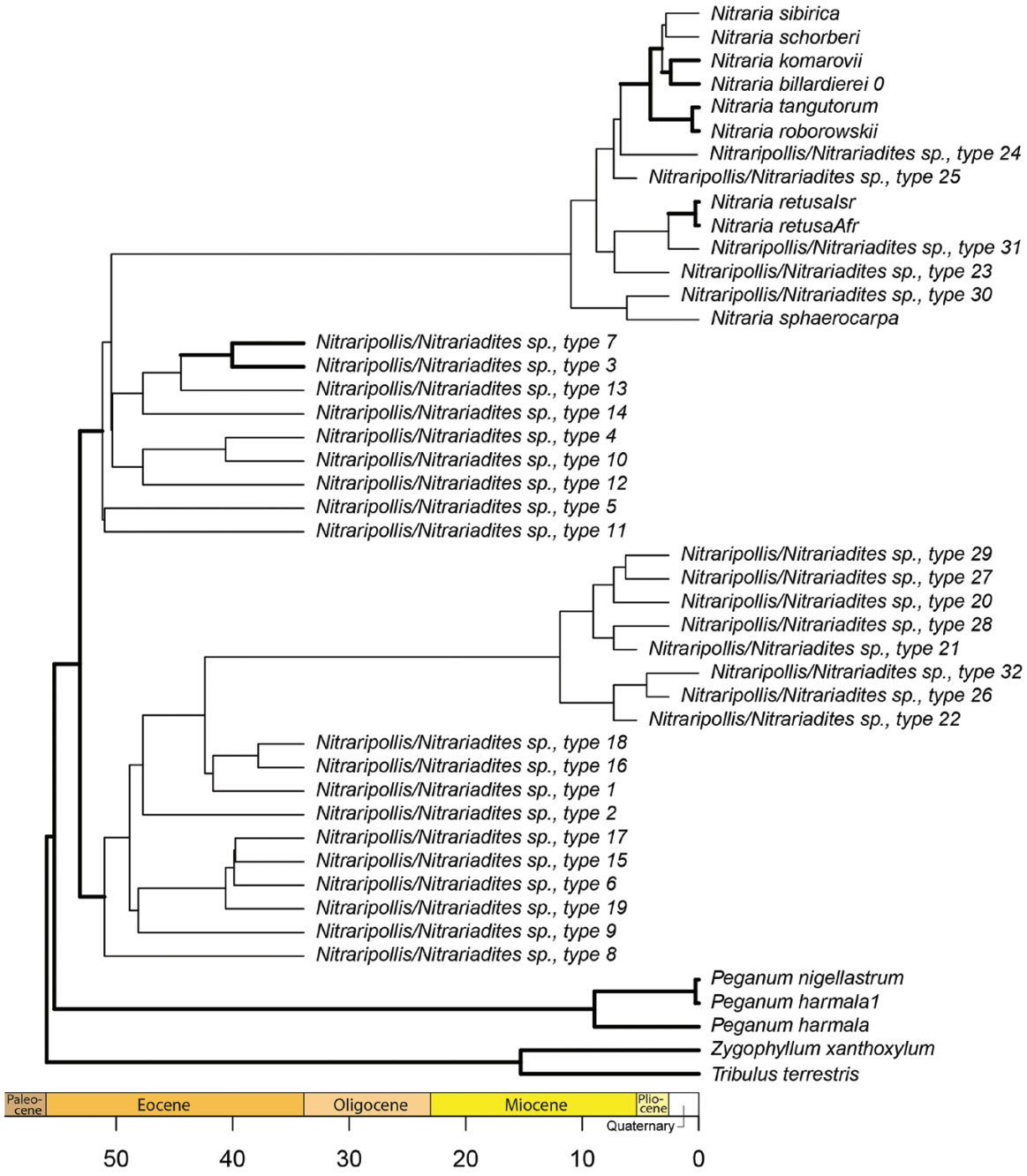

Figure 6. Total evidence phylogeny based on molecular data of the extant species and morphological data of the modern and fossil (morpho)species. Fossil ages are based on pollen occurrences in the fossil record. The phylogeny shows 32 fossil (extinct) morphospecies, 9 extant *Nitraria* species, 3 lineages of its sister genus *Peganum* and the outgroup with *Zygophyllum xanthoxylum* and *Tribulus terrestris*. Thick lines are used for branches with a posterior probability of >0.95. The highest diversity of *Nitraria* was reached in the Eocene, followed by a collapse at the Eocene-Oligocene Transition (EOT). Diversification occurred from the mid-Miocene onwards and extant species originate during the Late Miocene.

followed by a collapse at the EOT, when all but two of the sampled lineages went extinct (Fig. 7). This coincided with a severe cooling event, which formed the culmination of a long-term global cooling trend (Fig. 7). At the same time, atmospheric CO_2 decreased and the proto-Paratethys Sea fully retreated from Central Asia (Fig. 7). Due to a lack of pollen morphological data from Mid- and Late Oligocene deposits, diversification dynamics remain unknown for this epoch. The collapse in diversity might therefore be an over-estimation,

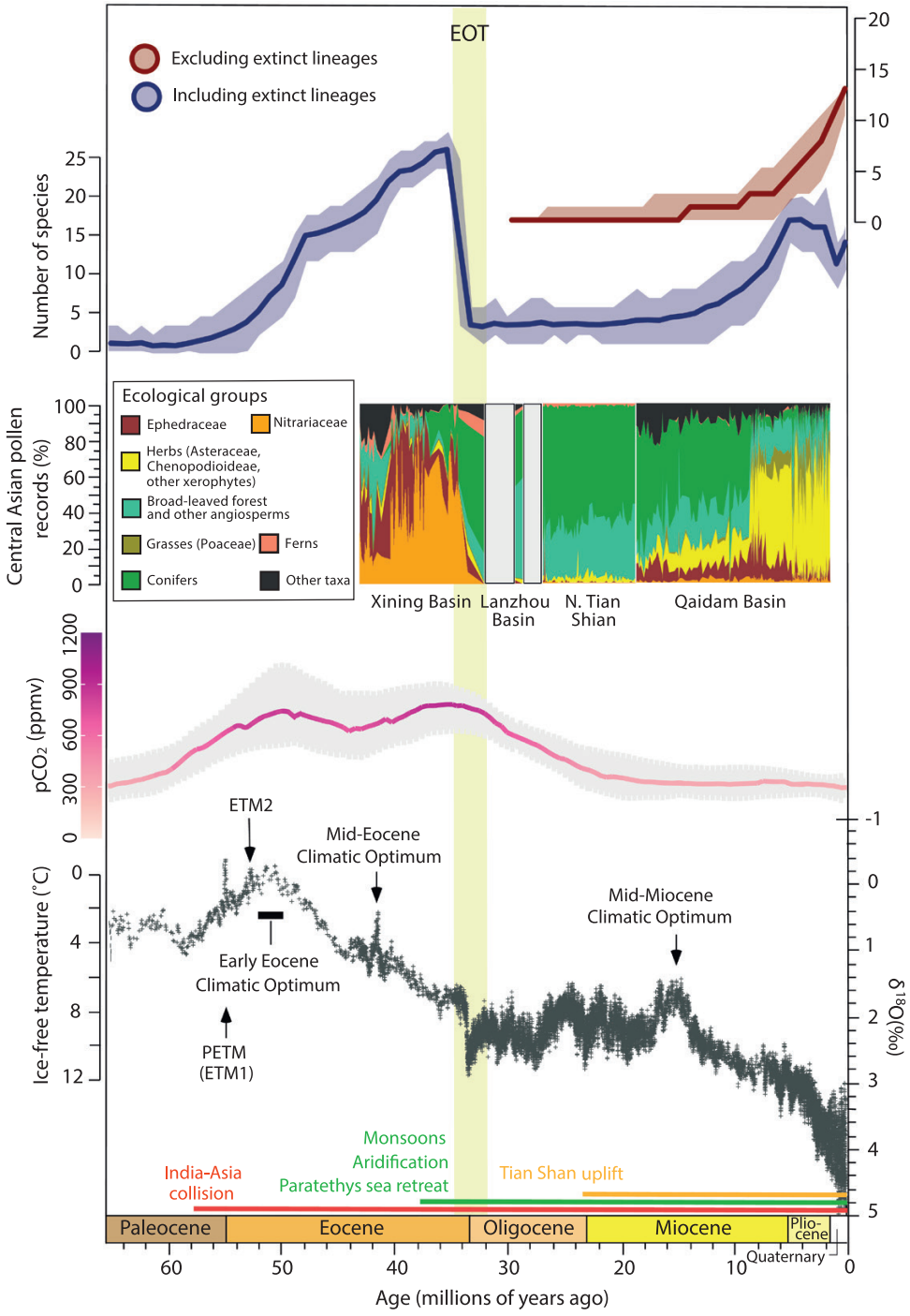

Figure 7. *Nitraria* diversity [number of (morpho)species] plotted through time and linked to climatic events, showing the collapse in diversity at the Eocene-Oligocene Transition (EOT). The graph shows deep-sea temperature, based on $\delta^{18}O$ values (Zachos *et al.*, 2008); atmospheric CO_2 (pCO_2; Foster *et al.*, 2017); the India-Asia collision (Hu *et al.*, 2016); the retreat of the Paratethys Sea (Bosboom *et al.*, 2011); and uplift of the Tian Shan. *Nitraria* diversity drastically decreased simultaneously with temperature and pCO_2 at the EOT, and just before the Paratethys Sea makes its final retreat west of Central Asia.

but Central Asian pollen records show that *Nitraria* remains virtually absent during the Oligocene (Fig. 7). Such a large drawback in abundance is likely to have also negatively impacted the diversity. *Nitraria* appears again in the pollen records in the Miocene, and according to the LTT plots, *Nitraria* diversity

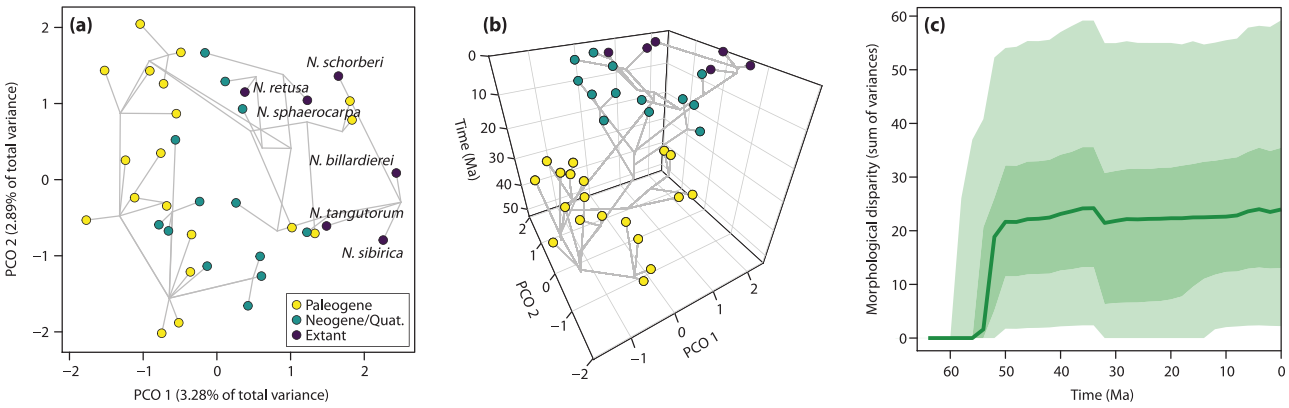

Figure 8. Phylomorphospace and morphological disparity of extant and fossil *Nitraria* pollen. A, Phylomorphospace (first two axes of a principal coordinates analysis), with points coloured by time period. Names of extant taxa are given for reference. B, Chronophylomorphospace, showing the morphological evolution of *Nitraria* through time. C, Morphological disparity through time, measured as the sums of variances of the ordination axes. The solid green line shows the median disparity calculated from a sample of 1600 posterior trees, the dark and light shaded regions show 50% and 95% confidence intervals, respectively.

increases again from the Mid-Miocene onwards, eventually leading to the origination of extant species. In contrast, the LTT plot based on the extant taxa shows the diversification event in the Miocene, but lacks any information on the older diversification of *Nitraria*. Thus, there is a stark difference between the diversity trajectory based on the full dataset and the trajectory based on extant taxa only, indicating contrasting representations of the evolutionary history of *Nitraria*.

Morphological disparity and the phylomorphospace

The first two axes of the phylomorphospace account for just over *c.* 7% of the variance in the data (Fig. 8a), with the remaining variance being spread over a further 71 axes. PCO1 corresponds to pollen size (smaller to larger along the axis), whereas PCO2 corresponds to pollen shape (more elongated at the lower end of the axis to more spherical at the upper end). The size gradient on PCO1 matches with a temporal gradient, with the Palaeogene taxa mostly occurring at the lower end of the axis and the extant taxa concentrated at the upper end of the axis, demonstrating a general increase in *Nitraria* pollen size over time. Adding on a third time axis (Fig. 8b) shows the loss of taxa from the record at the EOT, and the persistence of two lineages throughout the Oligocene, from which the morphospace is repopulated in the Miocene. The variance explained on the first two PCO axes is low, whereas higher ordination axes do not contain easily explainable signals (Supporting Information, Fig. S6), and alternative phylomorphospace construction approaches reveal a similar pattern to that presented here (cf. Fig. 8a; Supporting Information, Figs S4, S5), suggesting that this is the main morphological pattern present in the data.

The morphological disparity reconstruction has wide confidence intervals, reflecting the uncertainty in the phylogenetic estimation that is propagated through to the disparity calculation (Fig. 8c). Despite these uncertainties, this time series indicates that disparity rose quickly following the first appearance of *Nitraria*, and then remained broadly stable through to the present, with a possible slight decline at the Eocene-Oligocene boundary at *c.* 34 Mya.

DISCUSSION

Evolutionary history of *Nitraria*

The first appearance of *Nitraria* is thought to have occurred between the Cretaceous and the Early Palaeocene (Zhang *et al.*, 2015). Zhang *et al.* (2015) proposed a Palaeocene split between *N. sphaerocarpa* and the other lineages. However, in our study the oldest fossil had a minimum age of the Early Eocene (>53 Myr). Notably, the inclusion of fossil data in our study prompts us to challenge previous divergence time estimates, as the total evidence approach suggests the split between *N. sphaerocarpa* and the other lineages did not happen before the Miocene. The integration of the fossil record thus leads to a substantial reassessment of the origin and divergence times of the clade, as well as a complete reinterpretation of its diversification pattern.

Our results support the existing hypothesis that states that the area of origin of *Nitraria* is situated in

Central Asia (Zhang *et al.*, 2015). Zhang *et al.* (2015) specifically proposed the coastal eastern Tethys area as the place of origin, where the oldest fossil found in our study occurred in non-coastal deposits. This does not contradict the original hypothesis of an eastern Tethys origin, as coastal deposits from the Tarim Basin (41–37 Mya) did also contain fossil *Nitraria* pollen. Future investigation of older samples from the eastern Tethys region should demonstrate whether *Nitraria* pollen are also present in older marine deposits.

The LTT plots suggest a temporal correlation between the retreat of the Paratethys Sea out of Central Asia (Kaya *et al.*, 2019), simultaneous global cooling and inland aridification (Dupont-Nivet *et al.*, 2007), and a large reduction in the abundance and diversity of *Nitraria*. This large decrease in diversity just after the EOT is also concurrent with the disappearance of Central Asian salt deposits (Dupont-Nivet *et al.*, 2007; Ao *et al.*, 2020; Wang *et al.*, 2021) and part of a turnover in steppe vegetation in Central Asia (shown in Early Oligocene records; Barbolini *et al.*, 2020). Although the magnitude of the decline in diversity of *Nitraria* needs to be further examined (by filling in the missing gaps in pollen morphological measurements in the Oligocene), the timing of events is striking. Furthermore, its central role in this turnover makes *Nitraria* crucial in understanding the evolution of the Central Asian steppe biome. However, it remains difficult to determine the contribution of climatic drivers such as temperature, aridification and sea retreat to the major evolutionary bottleneck of *Nitraria*. Aridification leading to a hyper-arid, desert environment might have diminished suitable habitats (Barbolini *et al.*, 2020), the geographical extension and the fluctuations of the Paratethys Sea probably influenced dispersal patterns (Rögl, 1997; Manafzadeh *et al.*, 2017), and the opening and closing of the Turgai Strait (Akhmetsev & Beniamovski, 2006; Kaya *et al.*, 2019) could have promoted allopatric speciation. The records studied here are not sufficient to answer these questions, but future research could provide a first step by, for example, analysing niche evolution of *Nitraria* through time [as was done for *Potentilla* L. in Töpel *et al.* (2012)] in response to Palaeogene climate dynamics.

In the Miocene, renewed diversification gave rise to the modern species of *Nitraria*. This more recent origination of the extant *Nitraria* spp. would suggest that the Palaeogene fossils from this study belonged to now-extinct sister lineages, a pattern also observed for another Tibetan steppe taxon, *Ephedra* Tourn. ex L. (Rydin *et al.*, 2004). Although morphological disparity remained stable, *Nitraria* never regained its Eocene level of diversity, and we now know that the modern species reflect only a fraction of the diversity that once was (Figs 6, 7). Taxonomic diversity and morphological disparity tend to be decoupled (Foote, 1991), and this is exhibited in our data both in the rapid increase in disparity relative to the gradual rise in diversity early in *Nitraria* evolutionary history, and the apparent stability in disparity across the EOT and through to the present (although the high uncertainty in our disparity reconstruction makes this challenging to assess; Fig. 8c). Similarly, taxonomic diversification in the Miocene did not lead to morphological innovation, at least in pollen which might be more morphologically conserved than other plant traits (Fig. 8c). Our results also suggest that phylogenetic error propagation leads to higher uncertainty in morphological disparity estimates compared to taxonomic diversity (compare the 95% confidence intervals in Figs 7, 8c).

We should stress that extinct clades can have a different climatic envelope when compared to the modern species (as is the case for fossil *Mauritiidites* van Hoeken-Klinkenberg, 1964 taxa compared to the extant *Mauritia* L.f.; Bogota-Angel *et al.*, 2021). However, in the case of *Nitraria* the geological evidence suggests that both fossil and modern species preferred similar climatic and environmental conditions. The extant species occur in arid, saline areas near lake, coastal or playa environments (Perveen & Qaiser, 2006; Woutersen *et al.*, 2018), and, as explained above, these are conditions that resemble the settings in which fossil species thrived. Nevertheless, it remains unknown if these environmental preferences are linked to any of the pollen morphological features. Correlations between climate and pollen morphology have been found before (Ejsmond *et al.*, 2011; Lechowicz *et al.*, 2020), and *Ephedra* forms a striking example for the Central Asian region (Han *et al.*, 2016). Han *et al.* (2016) documented *Ephedra* pollen morphology through LM and SEM and suggest that the development of branched pseudosulci in *Ephedra* pollen occurred in response to aridification at the EOT. This is morphological innovation that might be associated with a change in pollination syndrome (Bolinder *et al.*, 2015). As for *Ephedra*, there could be specific pollen features (e.g. the perforated or non-perforated exine observed in both fossil and modern pollen) in *Nitraria* that might be linked to climatic circumstances, and could elucidate if extinction was random (acting on all species) or systematic (acting on species with specific morphological features). To find the link between pollen morphology and climate and to explain the evolutionary success of surviving lineages, more fossil pollen grains of *Nitraria* should be documented through high-quality imaging, such as SEM.

Limitations of the fossil record and phylogenetic analyses

Studying the pollen morphology of extant species is essential for resolving phylogenetic issues and characterizing species (Via do Pico & Dematteis, 2013; Tuler *et al.*, 2017). For *Nitraria*, studying pollen

morphology is an excellent way to differentiate modern species, since the morphological characteristics follow the phylogeny and thus reflect the genetic diversity within the genus (Woutersen *et al.*, 2018). However, with no phylogenetic context available, separating 'species' in the fossil record is challenging. The methodology used in this study focused on key pollen morphological characters, and assigned pollen grains to specific morphospecies based on the measurement or presence/absence of these characters, following the example of e.g. Oswald *et al.* (2011) and Tuler *et al.* (2017). Clear morphospecies can be distinguished, but with the morphological variation in the fossil pollen grains of *Nitraria* being gradual (particularly in the Eocene), morphospecies are connected by a range of transitions and a high taxonomic resolution is difficult to obtain. This might be improved in future work by closely documenting specific morphological features (e.g. the exine; Mander & Punyasena, 2014), through the use of new imaging techniques (e.g. high-resolution imaging such as SEM and Airyscan confocal microscopy) and methodological advances in machine learning (e.g. computational image analysis; Mander & Punyasena, 2014; Astolfi *et al.*, 2020; Romero *et al.*, 2020).

Other, more common difficulties in studying evolutionary histories are biased data (Raia *et al.*, 2013), lack of statistical power (Silvestro *et al.*, 2014), failure to meet the underlying model assumptions (Liow *et al.*, 2010; Coiro *et al.*, 2019), dating errors and taxonomic inconsistencies (Silvestro *et al.*, 2018), and the incompleteness of the fossil record (Lieberman, 2002). These issues are all possible causes for the disagreement between fossil and phylogenetic analyses. However, a main benefit of the approach taken here is that not only can evolutionary relationships using both extant and fossil taxa be analysed, and values derived from the phylogeny calculated (e.g. lineages through time, diversification rates), but the information can also be used for further downstream analyses to measure derived quantities such as morphological disparity through a continuous time series, including full propagation of phylogenetic uncertainty via a sample of posterior trees. Their joint inclusion leads, despite the natural limitations of the fossil record and phylogenetic analyses, to evolutionary studies with a higher accuracy (Donoghue *et al.*, 1989; Lieberman, 2002; Fritz *et al.*, 2013; Hopkins *et al.*, 2018; Fraser *et al.*, 2020).

Importance of total evidence approach in reconstructing evolutionary history

The combination of fossil and molecular data has often been used, usually to constrain the timing of origin or divergence time estimates (Ronquist *et al.*, 2012; Gavryushkina *et al.*, 2016), to document character evolution within species (Eklund *et al.*, 2004), and to reconstruct past biogeography (Cook & Crisp, 2005; Wood *et al.*, 2013). Fossil data are essential for the calibration of molecular datasets and provide fundamental evidence for timescales of origins and divergences (Donoghue *et al.*, 1989; Quental & Marshall, 2010; Coiro *et al.*, 2019). However, the fossil and molecular record do not always agree, and an extensive debate about the discrepancy between the two exists (Lieberman, 2002; Quental & Marshall, 2010; Silvestro *et al.*, 2018, 2021; Coiro *et al.*, 2019).

This study is a striking example of such a discrepancy (Fig. 7) and showcases the importance of including fossils in plant evolutionary studies. This holds for many other plant taxa and has been demonstrated, for example, for *Ephedra* (Rydin *et al.*, 2004), tree ferns (Soltis *et al.*, 2002), Betulaceae (Forest *et al.*, 2005), and Annonaceae and Myristicaceae (Doyle *et al.*, 2004). However, the problem has also been reported for non-plant species (e.g. Quental & Marshall, 2010; Ronquist *et al.*, 2012; Gavryushkina *et al.*, 2016; Herrera, 2017; Silvestro *et al.*, 2019), indicating that the discontinuity between the molecular and fossil record is widely spread amongst evolutionary studies from all fields.

The new historical perspective presented here adds to the current understanding of the evolution of the plant *Nitraria*. The inclusion of multiple fossil lineages in the analyses using the integrated framework provided by the fossilized birth-death model shows that the Palaeogene (Paratethys) sea retreat, aridification, climatic cooling and the disappearance of high-salinity environments were likely determinant in the evolutionary history of the genus. Our analyses lead to a reassessment of the diversification pattern of *Nitraria* and show that modern diversity is the result of a long evolutionary history. We view this as an exemplar case for the need and power of integrating fossil, morphometric and molecular data into total evidence phylogenies to fully understand plant evolution.

ACKNOWLEDGEMENTS

A.W., G.D-N. and N.M. acknowledge funding from European Research Council consolidator grant Monsoons in Asia caused Greenhouse to Icehouse Cooling (MAGIC) 649081. C.H. was supported by CAS President's International Fellowship Initiative Grant No. 2018VBA0038. D.S. received funding from the Swiss National Science Foundation (PCEFP3_187012; FN-1749) and from the Swedish Research Council (VR: 2019-04739). A.A. is supported by grants from the Swedish Foundation for Strategic Research, the

Swedish Research Council and the Royal Botanic Gardens, Kew. P.E.J. and A.K. received funding from the German Research Foundation (DFG grants 443701866 and KO4960/4). We thank Jan van Arkel for providing us with high quality microphotography and Huasheng Huang for SEM photography of fossil *Nitraria*. Furthermore, we thank Malcolm Jones of PLS PalyLab and Annemarie Philip from the University of Amsterdam for the preparation of palynological slides.

REFERENCES

Abbott LB, **Lepak D**, **Daniel DL. 2007**. Vegetative and reproductive phenology of African rue (*Peganum harmala*) in the northern Chihuahuan desert. *The Southwestern Naturalist* **52**: 209–218.

Abdusalih N, **Xiaoling P. 2003**. Pollen morphology and taxonomy of *Nitraria* and its allied genera in West China. *Arid Zone Research* **20**: 16–19.

Abels HA, **Dupont-Nivet G**, **Xiao G**, **Bosboom R**, **Krijgsman W. 2011**. Step-wise change of Asian interior climate preceding the Eocene-Oligocene Transition (EOT). *Palaeogeography, Palaeoclimatology, Palaeoecology* **299**: 399–412.

Agababian VSh, **Tumanian KT. 1972**. On pollen morphology of the genus *Nitraria* L. *Biol. Zh. Arm.*

Akhmets'ev MA, **Beniamovski VN. 2006**. The Paleocene and Eocene in the Russian part of West Eurasia. *Stratigraphy and Geological Correlation* **14**: 49–72.

Ao H, **Dupont-Nivet G**, **Rohling EJ**, **Zhang P**, **Ladant JB**, **Roberts AP**, **Licht A**, **Liu Q**, **Liu Z**, **Dekkers MJ**, **Coxall HK**, **Jin Z**, **Huang C**, **Xiao G**, **Poulsen CJ**, **Barbolini N**, **Meijer N**, **Sun Q**, **Qiang X**, **Yao J**, **An Z. 2020**. Orbital climate variability on the northeastern Tibetan Plateau across the Eocene-Oligocene transition. *Nature Communications* **11**: 1–11.

Astolfi G, **Gonçalves AB**, **Menezes GV**, **Borges FSB**, **Astolfi ACMN**, **Matsubara ET**, **Alvarez M**, **Pistori H. 2020**. POLLEN73S: an image dataset for pollen grains classification. *Ecological Informatics* **60**: 101165.

Barba-Montoya J, **dos Reis M**, **Schneider H**, **Donoghue PCJ**, **Yang Z. 2018**. Constraining uncertainty in the timescale of angiosperm evolution and the veracity of a Cretaceous terrestrial revolution. *New Phytologist* **218**: 819–834.

Barbolini N, **Woutersen A**, **Dupont-Nivet G**, **Silvestro D**, **Tardif D**, **Coster PMC**, **Meijer N**, **Chang C**, **Zhang HX**, **Licht A**, **Rydin C**, **Koutsodendris A**, **Han F**, **Rohrmann A**, **Liu XJ**, **Zhang Y**, **Donnadieu Y**, **Fluteau F**, **Ladant JB**, **Le Hir G**, **Hoorn C. 2020**. Cenozoic evolution of the steppe-desert biome in Central Asia. *Science Advances* **6**: eabb8227.

Bercovici A, **Hadley A**, **Villanueva-Amadoz U. 2009**. Improving depth of field resolution for palynological photomicrography. *Palaeontologia Electronica* **12**: 1–12.

Bessais E, **Cravatte J. 1988**. Les écosystèmes végétaux Pliocènes de Catalogne méridionale. Variations latitudinales dans le domaine nord-ouest méditerranéen. *Geobios* **21**: 49–63.

Bogota-Angel G, **Huang H**, **Jardine PE**, **Chazot N**, **Salamanca S**, **Banks H**, **Pardo-Trujillo A**, **Plata A**, **Dueñas H**, **Star W**, **Langelaan R**, **Eisawi A**, **Umeji OP**, **Enuenwemba LO**, **Parmar S**, **Rocha da Silveira R**, **Lim JY**, **Prasad V**, **Morley RJ**, **Bacon CD**, **Hoorn C. 2021**. Climate and geological change as drivers of Mauritiinae palm biogeography. *Journal of Biogeography* **48**: 1001–1022.

Bolinder K, **Niklas KJ**, **Rydin C. 2015**. Aerodynamics and pollen ultrastructure in *Ephedra*. *American Journal of Botany* **102**: 457–470.

Bosboom RE, **Abels HA**, **Hoorn C**, **van den Berg BCJ**, **Guo ZJ**, **Dupont-Nivet G. 2014**. Aridification in continental Asia after the Middle Eocene Climatic Optimum (MECO). *Earth and Planetary Science Letters* **389**: 34–42.

Bosboom RE, **Dupont-Nivet G**, **Houben AJ**, **Brinkhuis H**, **Villa G**, **Mandic O**, **Stoica M**, **Zachariasse WJ**, **Guo Z**, **Li C**, **Krijgsman W. 2011**. Late Eocene sea retreat from the Tarim Basin (west China) and concomitant Asian paleoenvironmental change. *Palaeogeography, Palaeoclimatology, Palaeoecology* **299**: 385–398.

Bouckaert R, **Heled J**, **Kühnert D**, **Vaughan T**, **Wu CH**, **Xie D**, **Suchard MA**, **Rambaut A**, **Drummond AJ. 2014**. BEAST 2: a software platform for Bayesian evolutionary analysis. *PLoS Computational Biology* **10**: e1003537.

Bouchal JM, **Zetter R**, **Grímsson F**, **Denk T. 2016**. The middle Miocene palynoflora and palaeoenvironments of Eskihisar (Yatağan basin, south-western Anatolia): a combined LM and SEM investigation. *Botanical Journal of the Linnean Society* **182**: 14–79.

Bouchal JM, **Mayda S, Zetter R, Grímsson F, Akgün F, Denk T. 2017**. Miocene palynofloras of the Tınaz lignite mine, Muğla, southwest Anatolia: taxonomy, palaeoecology and local vegetation change. *Review of Palaeobotany and Palynology* **243**: 1–36.

Bougeois L, **Dupont-Nivet G**, **de Rafélis M**, **Tindall JC**, **Proust JN**, **Reichart GJ**, **de Nooijer LJ**, **Guo Z**, **Ormukov C. 2018**. Asian monsoons and aridification response to Paleogene sea retreat and Neogene westerly shielding indicated by seasonality in Paratethys oysters. *Earth and Planetary Science Letters* **485**: 99–110.

de Bruijn H, **Daams R**, **Daxner-Höck G**, **Fahlbusch V**, **Ginsburg L**, **Mein P**, **Morales J. 1990**. Report of the RCMNS working group on fossil mammals, Reisensburg. *Newsletters on Stratigraphy* **26**: 65–118.

Cai M, **Fang X**, **Wu F**, **Miao Y**, **Appel E. 2012**. Pliocene-Pleistocene stepwise drying of Central Asia: evidence from paleomagnetism and sporopollen record of the deep borehole SG-3 in the western Qaidam Basin, NE Tibetan Plateau. *Global and Planetary Change* **94**: 72–81.

Cailliez F. 1983. The analytical solution of the additive constant problem. *Psychometrika* **48**: 305–308.

Cavagnetto C, **Anadón P. 1996**. Preliminary palynological data on floristic and climatic changes during the Middle Eocene-Early Oligocene of the eastern Ebro Basin, northeast Spain. *Review of Palaeobotany and Palynology* **92**: 281–305.

Coiro M, **Doyle JA**, **Hilton J. 2019**. How deep is the conflict between molecular and fossil evidence on the age of angiosperms? *New Phytologist* **223**: 83–99.

Cook LG, **Crisp MD. 2005**. Not so ancient: the extant crown group of *Nothofagus* represents a post-Gondwanan radiation. *Proceedings of the Royal Society B: Biological Sciences* **272**: 2535–2544.

Coxall HK, **Wilson PA**, **Pälike H**, **Lear CH**, **Backman J. 2005**. Rapid stepwise onset of Antarctic glaciation and deeper calcite compensation in the Pacific Ocean. *Nature* **433**: 53–57.

Crisp MD, **Cook LG**, **Bowman DMJS**, **Cosgrove M**, **Isagi Y**, **Sakaguchi S. 2019**. Turnover of southern cypresses in the post-Gondwanan world: extinction, transoceanic dispersal, adaptation and rediversification. *New Phytologist* **221**: 2308–2319.

Dai S, **Fang X**, **Dupont-Nivet G**, **Song C**, **Gao J**, **Krijgsman W**, **Langereis C**, **Zhang W. 2006**. Magnetostratigraphy of Cenozoic sediments from the Xining Basin: tectonic implications for the northeastern Tibetan Plateau. *Journal of Geophysical Research: Solid Earth* **111**: 1–19.

DeConto RM, **Pollard D. 2003**. Rapid Cenozoic glaciation of Antarctica induced by declining atmospheric CO_2. *Nature* **421**: 245–249.

Denk T, **Güner HT**, **Bouchal JM. 2019**. Early Miocene climate and biomes of Turkey: Evidence from leaf fossils, dispersed pollen, and petrified wood. *Palaeogeography, Palaeoclimatology, Palaeoecology* **530**: 236–248.

Donoghue MJ, **Doyle JA**, **Gauthier J**, **Kluge AG**, **Rowe T. 1989**. The importance of fossils in phylogeny reconstruction. *Annual Review of Ecology and Systematics* **20**: 431–460.

Doyle JA, **Sauquet H**, **Scharaschkin T**, **Le Thomas A. 2004**. Phylogeny, molecular and fossil dating, and biogeographic history of Annonaceae and Myristicaceae (Magnoliales). *International Journal of Plant Sciences* **165**: S55–S67.

Duan QF, **Zhang KX**, **Wang JX**, **Yao HZ**, **Pu JJ. 2007**. Sporopollen assemblage from the Totohe Formation and its stratigraphic significance in the Tanggula Mountains, northern Tibet. *Earth Science Journal - Journal of China University of Geosciences* **32**: 623–637.

Dupont-Nivet G, **Hoorn C**, **Konert M. 2008**. Tibetan uplift prior to the Eocene-Oligocene climate transition: evidence from pollen analysis of the Xining Basin. *Geology* **36**: 987.

Dupont-Nivet G, **Hoorn C**, **Konert M. 2009**. Erratum. *Geology* **37**: 506.

Dupont-Nivet G, **Krijgsman W**, **Langereis CG**, **Abels HA**, **Dai S**, **Fang X. 2007**. Tibetan Plateau aridification linked to global cooling at the Eocene-Oligocene Transition. *Nature* **445**: 635–638.

Ejsmond MJ, **Wrońska-Pilarek D**, **Ejsmond A**, **Dragosz-Kluska D**, **Karpińska-Kołaczek M**, **Kołaczek P**, **Kozłowski J. 2011**. Does climate affect pollen morphology? Optimal size and shape of pollen grains under various desiccation intensity. *Ecosphere* **2**: art117.

Eklund H, **Doyle JA**, **Herendeen PS. 2004**. Morphological phylogenetic analysis of living and fossil Chloranthaceae. *International Journal of Plant Sciences* **165**: 107–151.

Ersoy EY, **Çemen İ**, **Helvacı C**, **Billor Z. 2014**. Tectono-stratigraphy of the Neogene basins in Western Turkey: Implications for tectonic evolution of the Aegean Extended Region. *Tectonophysics* **635**: 33–58.

Foote M. 1991. *Morphological and taxonomic diversity in a clade's history: the blastoid record and stochastic simulations*. Ann Arbor: Museum of Paleontology, University of Michigan.

Forest F, **Savolainen V**, **Chase MW**, **Lupia R**, **Bruneau A**, **Crane PR. 2005**. Teasing apart molecular- versus fossil-based error estimates when dating phylogenetic trees: a case study in the birch family (Betulaceae). *Systematic Botany* **30**: 118–133.

Foster GL, **Royer DL**, **Lunt DJ. 2017**. Future climate forcing potentially without precedent in the last 420 million years. *Nature Communications* **8**: 1–8.

Fraser D, **Soul LC**, **Tóth AB**, **Balk MA**, **Eronen JT**, **Pineda-Munoz S**, **Shupinski AB**, **Villaseñor A**, **Barr WA**, **Behrensmeyer AK**, **Du A**, **Faith JT**, **Gotelli NJ**, **Graves GR**, **Jukar AM**, **Looy CV**, **Miller JH**, **Potts R**, **Lyons SK. 2020**. Investigating biotic interactions in deep time. *Trends in Ecology & Evolution* **36**: 61–75.

Fritz SA, **Schnitzler J**, **Eronen JT**, **Hof C**, **Böhning-Gaese K**, **Graham CH. 2013**. Diversity in time and space: wanted dead and alive. *Trends in Ecology & Evolution* **28**: 509–516.

Garnier S, **Ross N**, **Rudis R**, **Camargo AP**, **Sciaini M**, **Scherer C. 2021**. *Rvision - colorblind-friendly color maps for R. R package version 0.6.1*.

Gavryushkina A, **Heath TA**, **Ksepka DT**, **Stadler T**, **Welch D**, **Drummond AJ. 2016**. Bayesian total-evidence dating reveals the recent crown radiation of penguins. *Systematic Biology* **60**: 57–73.

Guillerme T. 2018. dispRity: a modular R package for measuring disparity. *Methods in Ecology and Evolution* **9**: 1755–1763.

Guillerme T, **Cooper N. 2018**. Time for a rethink: time sub-sampling methods in disparity-through-time analyses. *Palaeontology* **61**: 481–493.

Halbritter H, **Ulrich S**, **Grímsson F**, **Weber M**, **Zetter R**, **Hesse M**, **Buchner R**, **Svojtka M**, **Frosch-Radivo A. 2018**. *Illustrated pollen terminology*. Cham: Springer.

Han F, **Rydin C**, **Bolinder K**, **Dupont-Nivet G**, **Abels HA**, **Koutsodendris A**, **Zhang K**, **Hoorn C. 2016**. Steppe development on the northern Tibetan Plateau inferred from Paleogene ephedroid pollen. *Grana* **55**: 71–100.

Heath TA, **Huelsenbeck JP**, **Stadler T. 2014**. The fossilized birth-death process for coherent calibration of divergence-time estimates. *Proceedings of the National Academy of Sciences, USA* **111**: E2957–E2966.

Herb C, **Appel E**, **Voigt S**, **Koutsodendris A**, **Pross J**, **Zhang W**, **Fang X. 2015**. Orbitally tuned age model for the Late Pliocene-Pleistocene lacustrine succession of drill core SG-1 from the western Qaidam Basin (NE Tibetan Plateau). *Geophysical Journal International* **200**: 35–51.

Herrera JP. 2017. Primate diversification inferred from phylogenies and fossils. *Evolution* **71**: 2845–2857.

Hoorn C, **Straathof J**, **Abels HA**, **Xu Y**, **Utescher T**, **Dupont-Nivet G. 2012**. A Late Eocene palynological record of climate change and Tibetan Plateau uplift (Xining Basin, China). *Palaeogeography, Palaeoclimatology, Palaeoecology* **344**: 16–38.

Hopkins MJ, **Bapst DW**, **Simpson C**, **Warnock RCM. 2018**. The inseparability of sampling and time and its influence on attempts to unify the molecular and fossil records. *Paleobiology* **44**: 561–574.

Houben AJP, **Bijl PK**, **Guerstein GR**, **Sluijs A**, **Brinkhuis H. 2011**. *Malvinia escutiana*, a new biostratigraphically important Oligocene dinoflagellate cyst from the Southern Ocean. *Review of Palaeobotany and Palynology* **165**: 175–182.

Hunt G, **Slater G. 2016**. Integrating paleontological and phylogenetic approaches to macroevolution. *Annual Review of Ecology, Evolution, and Systematics* **47**: 189–213.

Hu X, **Garzanti E**, **Wang J**, **Huang W**, **An W**, **Webb A. 2016**. The timing of India-Asia collision onset–Facts, theories, controversies. *Earth-Science Reviews* **160**: 264–299.

Kaya O, **Ünay E**, **Göktaş F**, **Saraç G. 2007**. Early Miocene stratigraphy of central west Anatolia, Turkey: implications for the tectonic evolution of the eastern Aegean area. *Geological Journal* **42**: 85–109.

Kaya MY, **Dupont-Nivet G**, **Proust J**, **Roperch P**, **Bougeois L**, **Meijer N**, **Frieling J**, **Fioroni C**, **Özkan Altıner S**, **Vardar E**, **Barbolini N**, **Stoica M**, **Aminov J**, **Mamtimin M**, **Zhaojie G. 2019**. Paleogene evolution and demise of the proto-Paratethys Sea in Central Asia (Tarim and Tajik basins): role of intensified tectonic activity at ca. 41 Ma. *Basin Research* **31**: 461–486.

Koutsodendris A, **Allstädt FJ**, **Kern OA**, **Kousis I**, **Schwarz F**, **Vannacci M**, **Woutersen A**, **Appel E**, **Berke MA**, **Fang X**, **Friedrich O**, **Hoorn C**, **Salzmann U**, **Pross J. 2019**. Late Pliocene vegetation turnover on the NE Tibetan Plateau (Central Asia) triggered by early Northern Hemisphere glaciation. *Global and Planetary Change* **180**: 117–125.

Koutsodendris A, **Sachse D**, **Appel E**, **Herb C**, **Fischer T**, **Fang X**, **Pross J. 2018**. Prolonged monsoonal moisture availability preconditioned glaciation of the Tibetan Plateau during the Mid-Pleistocene transition. *Geophysical Research Letters* **45**: 13–20.

Larrasoaña JC, **González-Delgado JA**, **Civis J**, **Sierro FJ**, **Alonso-Gavilán G**, **Pais J. 2008**. Magnetobiostratigraphic dating and environmental magnetism of Late Neogene marine sediments recovered at the Huelva-1 and Montemayor-1 boreholes (lower Guadalquivir Basin, Spain). *Geo-Temas* **10**: 1175–1178.

Lechowicz K, **Dyderski MK**, **Wrońska-Pilarek D. 2020**. How much of morphological variability in pollen from genus *Rubus* L. might be explained by climate variability. *Webbia* **75**: 305–315.

Lewis PO. 2001. A likelihood approach to estimating phylogeny from discrete morphological character data. *Systematic Biology* **50**: 913–925.

Li JX, **Yue LP**, **Roberts AP**, **Hirt AM**, **Pan F**, **Guo L**, **Xu Y**, **Xi RG**, **Guo L**, **Qiang XK**, **Gai CC**, **Jiang ZX**, **Sun ZM**, **Liu QS. 2018**. Global cooling and enhanced Eocene Asian mid-latitude interior aridity. *Nature Communications* **9**: 1–8.

Lieberman BS. 2002. Phylogenetic biogeography with and without the fossil record: gauging the effects of extinction and paleontological incompleteness. *Palaeogeography, Palaeoclimatology, Palaeoecology* **178**: 39–52.

Liow LH, **Quental TB**, **Marshall CR. 2010**. When can decreasing diversification rates be detected with molecular phylogenies and the fossil record? *Systematic Biology* **59**: 646–659.

Lloyd GT. 2016. Estimating morphological diversity and tempo with discrete character-taxon matrices: implementation, challenges, progress, and future directions. *Biological Journal of the Linnean Society* **118**: 131–151.

Lloyd GT. 2018. Journeys through discrete-character morphospace: synthesizing phylogeny, tempo, and disparity. *Palaeontology* **61**: 637–645.

López-Martínez N, **Agustí J**, **Cabrera L**, **Calvo Sorando JP**, **Civis J**, **Corrochano A**, **Daams R**, **Díaz-Esteban M**, **Elizaga E**, **Hoyos-Gómez M**, **Martínez J**, **Morales J**, **Portero JM**, **Robles F**, **de Santisteban C**, **José de Torres T**, **Alberdi MT**, **Álvarez M**, **Belinchón M**, **Carballeira J**, **Cuenca G**, **Freudenthal M**, **García E**, **Gibert J**, **González A**, **Junco F**, **Lacomba JI**, **Mazo AV**, **van der Meulen AJ**, **Moyà-Solà S**, **Olivé A**, **Ordoñez S**, **Renzi M**, **Sacristán MA**, **Sesé C**, **Soria D**, **Usera J**, **Zapata JL. 1985**. Approach to the Spanish continental Neogene synthesis and paleoclimatic interpretation. VIIIth Congress of the Regional Committee on Mediterranean Neogene Stratigraphy, Abstracts, Budapest, 348–350.

Louca S, **Pennell MW. 2020**. Extant timetrees are consistent with a myriad of diversification histories. *Nature* **580**: 502–505.

Manafzadeh S, **Staedler YM**, **Conti E. 2017**. Visions of the past and dreams of the future in the Orient: the Irano-Turanian region from classical botany to evolutionary studies. *Biological Reviews* **92**: 1365–1388.

Mander L, **Punyasena SW. 2014**. On the taxonomic resolution of pollen and spore records of earth's vegetation. *International Journal of Plant Sciences* **175**: 931–945.

Manos PS, **Soltis PS**, **Soltis DE**, **Manchester SR**, **Oh SH**, **Bell CD**, **Dilcher DL**, **Stone DE. 2007**. Phylogeny of extant and fossil Juglandaceae inferred from the integration of molecular and morphological data sets. *Systematic Biology* **56**: 412–430.

Meijer N. 2021. *Asian dust, monsoons and westerlies during the Eocene*. Doctoral Dissertation, Universität Potsdam.

Meijer N, **Dupont-Nivet G**, **Licht A**, **Roperch P**, **Rohrmann A**, **Sun A**, **… & Nowaczyk N. 2022**. Early Eocene magnetostratigraphy and tectonic evolution of the Xining Basin, NE Tibet. *Basin Research*. doi:10.1111/bre.12720

Miao Y, **Fang X**, **Herrmann M**, **Wu F**, **Zhang Y**, **Liu D. 2011**. Miocene pollen record of KC-1 core in the Qaidam Basin, NE Tibetan Plateau and implications for evolution of the East Asian monsoon. *Palaeogeography, Palaeoclimatology, Palaeoecology* **299**: 30–38.

Miao Y, **Fang X**, **Liu YS (Christopher)**, **Yan X**, **Li S**, **Xia W. 2016**. Late Cenozoic pollen concentration in the western Qaidam Basin, northern Tibetan Plateau, and its significance for paleoclimate and tectonics. *Review of Palaeobotany and Palynology* **231**: 14–22.

Miao Y, **Wu F**, **Herrmann M**, **Yan X**, **Meng Q. 2013**. Late Early Oligocene East Asian summer monsoon in the NE Tibetan Plateau: evidence from a palynological record from the Lanzhou Basin, China. *Journal of Asian Earth Sciences* **75**: 46–57.

Mitchell JS, **Etienne RS**, **Rabosky DL. 2018**. Inferring diversification rate variation from phylogenies with fossils. *Systematic Biology* **68**: 1–18.

Nauheimer L, **Metzler D**, **Renner SS. 2012**. Global history of the ancient monocot family Araceae inferred with models accounting for past continental positions and previous ranges based on fossils. *New Phytologist* **195**: 938–950.

Oksanen J, **Blanchet FG**, **Friendly M**, **Kindt R**, **Legendre P**, **McGlinn D**, **Minchin PR**, **O'Hara RBO**, **Simpson GL**, **Solymos P**, **Stevens MHH**, **Szoecs E**, **Wagner H. 2020**. *vegan: community ecology package. R package version 2.5-7*. Available at: https://CRAN.R-project.org/package=vegan

Oswald WW, **Doughty ED**, **Ne'eman G**, **Ne'eman R**, **Ellison AM. 2011**. Pollen morphology and its relationship to taxonomy of the genus *Sarracenia* (Sarraceniaceae). *Rhodora* **113**: 235–251.

Pan XL, **Shen GM**, **Chen P. 1999**. A preliminary research on taxonomy and systematics genus *Nitraria*. *Plant Diversity* **21**: 1.

Paradis E, **Schliep K. 2019**. ape 5.0: an environment for modern phylogenetics and evolutionary analyses in R. *Bioinformatics* **35**: 526–528.

Perveen A, **Qaiser M. 2006**. Pollen flora of Pakistan - XLIX. Zygophyllaceae. *Pakistan Journal of Botany* **38**: 225–232.

Quental TB, **Marshall CR. 2010**. Diversity dynamics: molecular phylogenies need the fossil record. *Trends in Ecology & Evolution* **25**: 434–441.

R Core Team. **2021**. *R: a language and environment for statistical computing*. Vienna: R Foundation for Statistical Computing.

Raia P, **Carotenuto F**, **Passaro F**, **Piras P**, **Fulgione D**, **Werdelin L**, **Saarinen J**, **Fortelius M. 2013**. Rapid action in the Palaeogene, the relationship between phenotypic and taxonomic diversification in Coenozoic mammals. *Proceedings of the Royal Society B: Biological Sciences* **280**: 20122244.

Ricklefs RE. 2007. Estimating diversification rates from phylogenetic information. *Trends in Ecology & Evolution* **22**: 601–610.

Rodríguez-Fernández J, **Comas MC**, **Soría J**, **Martín-Pérez J**, **Soto J**, **Zahn R**, **Klaus A. 1999**. The sedimentary record of the Alboran Basin: an attempt at sedimentary sequence correlation and subsidence analysis. In: Zahn R, Comas MC, Klaus A, eds. *Proceedings of the Ocean Drilling Program, scientific results, Vol. 161*. Texas: Ocean Drilling Program, 69–71.

Rögl F. 1997. Palaeogeographic considerations for Mediterranean and Paratethys seaways (Oligocene to Miocene). *Annalen Des Naturhistorischen Museums in Wien. Serie A Für Mineralogie Und Petrographie, Geologie Und Paläontologie, Anthropologie Und Prähistorie* **99**: 279–310.

Romero IC, **Kong S**, **Fowlkes CC**, **Jaramillo C**, **Urban MA**, **Oboh-Ikuenobe F**, **D'Apolito C**, **Punyasena SW. 2020**. Improving the taxonomy of fossil pollen using convolutional neural networks and superresolution microscopy. *Proceedings of the National Academy of Sciences, USA* **117**: 28496–28505.

Ronquist F, **Klopfstein S**, **Vilhelmsen L**, **Schulmeister S**, **Murray DL**, **Rasnitsyn AP. 2012**. A total-evidence approach to dating with fossils, applied to the early radiation of the Hymenoptera. *Systematic Biology* **61**: 973–999.

Rydin C, **Pedersen KR**, **Friis EM. 2004**. On the evolutionary history of *Ephedra*: Cretaceous fossils and extant molecules. *Proceedings of the National Academy of Sciences, USA* **101**: 16571–16576.

Sakamoto M, **Ruta M. 2012**. Convergence and divergence in the evolution of cat skulls: temporal and spatial patterns of morphological diversity. *PLoS One* **7**: e39752.

Sidlauskas B. 2008. Continuous and arrested morphological diversification in sister clades of characiform fishes: a phylomorphospace approach. *Evolution* **62**: 3135–3156.

Silvestro D, **Bacon CD**, **Ding W**, **Zhang Q**, **Donoghue PCJ**, **Antonelli A**, **Xing Y. 2021**. Fossil data support a pre-Cretaceous origin of flowering plants. *Nature Ecology & Evolution* **5**: 449–457.

Silvestro D, **Schnitzler J**, **Liow LH**, **Antonelli A**, **Salamin N. 2014**. Bayesian estimation of speciation and extinction from incomplete fossil occurrence data. *Systematic Biology* **63**: 349–367.

Silvestro D, **Tejedor MF**, **Serrano-Serrano ML**, **Loiseau O**, **Rossier V**, **Rolland J**, **Zizka A**, **Höhna S**, **Antonelli A**, **Salamin N. 2019**. Early arrival and climatically-linked geographic expansion of New World monkeys from tiny African ancestors. *Systematic Biology* **68**: 78–92.

Silvestro D, **Warnock RCM**, **Gavryushkina A**, **Stadler T. 2018**. Closing the gap between palaeontological and neontological speciation and extinction rate estimates. *Nature Communications* **9**: 5237.

Slater GJ. 2015. Iterative adaptive radiations of fossil canids show no evidence for diversity-dependent trait evolution. *Proceedings of the National Academy of Sciences, USA* **112**: 4897–4902.

Soetaert KER. 2019. *plot3D: plotting multi-dimensional data. R package version 1.3*. Available at: https://CRAN.R-project.org/package=plot3D

Soltis PS, **Soltis DE**, **Savolainen V**, **Crane PR**, **Barraclough TG. 2002**. Rate heterogeneity among lineages of tracheophytes: integration of molecular and fossil data and evidence for molecular living fossils. *Proceedings of the National Academy of Sciences, USA* **99**: 4430–4435.

Su Z, **Lu W**, **Zhang M. 2016**. Phylogeographical patterns of two closely related desert shrubs, *Nitraria roborowskii* and *N. sphaerocarpa* (Nitrariaceae), from arid north-western China. *Botanical Journal of the Linnean Society* **180**: 334–347.

Temirbayeva K, **Zhang ML. 2015**. Molecular phylogenetic and biogeographical analysis of *Nitraria* based on nuclear and chloroplast DNA sequences. *Plant Systematics and Evolution* **301**: 1897–1906.

Töpel M, **Antonelli A**, **Yesson C**, **Eriksen B. 2012**. Past climate change and plant evolution in western North America: a case study in Rosaceae. *PLoS One* **7**: e50358.

Tuler AC, **da Silva T**, **Carrijo TT**, **Garbin ML**, **Mendonça CBF**, **Peixoto AL**, **Gonçalves-Esteves V. 2017**. Taxonomic significance of pollen morphology for species delimitation in *Psidium* (Myrtaceae). *Plant Systematics and Evolution* **303**: 317–327.

Via do Pico GM, **Dematteis M. 2013**. Pollen morphology and implications for the taxonomy of the genus *Chrysolaena* (Vernonieae, Asteraceae). *Palynology* **37**: 177–188.

Wang X, **Carrapa B**, **Sun Y**, **Dettman DL**, **Chapman JB**, **Caves Rugenstein JK**, **Clementz MT**, **DeCelles PG**, **Wang M**, **Chen J**, **Quade J**, **Wang F**, **Li Z**, **Oimuhammadzoda I**, **Gadoev M**, **Lohmann G**, **Zhang X**, **Chen F. 2020**. The role of the westerlies and orography in Asian hydroclimate since the Late Oligocene. *Geology* **48**: 728–732.

Wang DN, **Sun XY**, **Zhao YN. 1990b**. Late Cretaceous to tertiary palynofloras in Xinjiang and Qinghai, China. *Review of Palaeobotany and Palynology* **65**: 95–104.

Wang DN, **Sun XY**, **Zhao YN**, **He Z. 1990a**. *The study on the micropaleobotany from Cretaceous-Tertiary of the oil bearing basins in some regions of Qinghai and Xinjang*. Beijing: China Environmental Science Press.

Wang Y, **Yuan S**, **Zhang T**, **Liu X**, **Liu Y**, **Miao Y. 2021**. Sedimentary record of climate change across the Eocene/Oligocene transition from the Qaidam Basin, northeastern Tibetan Plateau. *Palaeogeography, Palaeoclimatology, Palaeoecology* **564**: 110203.

Warnes GR, **Bolker B**, **Lumley T. 2020**. *gtools: various R programming tools. R package version 3.8.2*. Available at: https://CRAN.R-project.org/package=gtools

Warnock RCM, **Heath TA**, **Stadler T. 2020**. Assessing the impact of incomplete species sampling on estimates of speciation and extinction rates. *Paleobiology* **46**: 137–157.

WCVP. **2023**. *World checklist of vascular plants*. Kew: Facilitated by the Royal Botanic Gardens.

Wood HM, **Matzke NJ**, **Gillespie RG**, **Griswold CE. 2013**. Treating fossils as terminal taxa in divergence time estimation reveals ancient vicariance patterns in the palpimanoid spiders. *Systematic Biology* **62**: 264–284.

Woutersen A, **Jardine PE**, **Bogotá-Angel RG**, **Zhang HX**, **Silvestro D**, **Antonelli A**, **Gogna E**, **Erkens RHJ**, **Gosling WD**, **Dupont-Nivet G**, **Hoorn C. 2018**. A novel approach to study the morphology and chemistry of pollen in a phylogenetic context, applied to the halophytic taxon *Nitraria* L. (Nitrariaceae). *PeerJ* **6**: e5055.

Xi Y, **Sun M. 1987**. Pollen morphology of *Nitraria* and its geological distribution. *Botanical Research (China)* **2**: 235–243.

Xi Y, **Zhang J. 1991**. The comparative studies of pollen morphology between *Nitraria* and Meliaceae. *Botanical Research (China)* **5**: 47–58.

Yin H, **Wang L**, **Shi Y**, **Qian C**, **Zhou H**, **Wang W**, **Ma XF**, **Tran LSP**, **Zhang B. 2020**. The East Asian winter monsoon acts as a major selective factor in the intraspecific differentiation of drought-tolerant *Nitraria tangutorum* in northwest China. *Plants* **9**: 1100.

Yu SX, **Janssens SB**, **Zhu XY**, **Lidén M**, **Gao TG**, **Wang W. 2016**. Phylogeny of *Impatiens* (Balsaminaceae): integrating molecular and morphological evidence into a new classification. *Cladistics* **32**: 179–197.

Zachos J, **Kump L. 2005**. Carbon cycle feedbacks and the initiation of Antarctic glaciation in the earliest Oligocene. *Global and Planetary Change* **47**: 51–66.

Zachos JC, **Dickens GR**, **Zeebe RE. 2008**. An early Cenozoic perspective on greenhouse warming and carbon-cycle dynamics. *Nature* **451**: 279–283.

Zetter J. 1989. Methodik und Bedeutung einer routinematig kombinierten lichtmikroskopischen und rasterelektronmikroskopischen Untersuchung Fossiler Mikrofloren. *Courier Forschungsinstitut Senckenberg* **109**: 41–50.

Zhang W, **Appel E**, **Fang X**, **Song C**, **Cirpka O. 2012**. Magnetostratigraphy of deep drilling core SG-1 in the western Qaidam Basin (NE Tibetan Plateau) and its tectonic implications. *Quaternary Research* **78**: 139–148.

Zhang W, **Appel E**, **Fang X**, **Song C**, **Setzer F**, **Herb C**, **Yan M. 2014**. Magnetostratigraphy of drill-core SG-1b in the western Qaidam Basin (NE Tibetan Plateau) and tectonic implications. *Geophysical Journal International* **197**: 90–118.

Zhang ML, **Temirbayeva K**, **Sanderson SC**, **Chen X. 2015**. Young dispersal of xerophil *Nitraria* lineages in intercontinental disjunctions of the Old World. *Scientific Reports* **5**: 1–8.

Zhao T, **Wang ZT**, **Branford-White CJ**, **Xu H**, **Wang CH. 2011**. Classification and differentiation of the genus *Peganum* indigenous to China based on chloroplast *trnL-F* and *psbA-trnH* sequences and seed coat morphology. *Plant Biology* **13**: 940–947.

Zunghao Z, **Ping W**, **Zhichen S**, **Yiyong Z. 1985**. *A research on tertiary palynological from the Qaidam Basin, Qinghai Province*. Beijing: Petroleum Industry Press.

SUPPORTING INFORMATION

Additional supporting information may be found in the online version of this article on the publisher's website.

Data S1. Geographical and climatic background.
Data S2. Descriptions of *Nitraria* and fossil *Nitraripollis/Nitrariadites* pollen.
Data S3. Morphological character data.
Data S4. Alignments for phylogenetic analysis from Zhang *et al.* (2015).
Figure S1. Boxplots showing the variability within the scored morphological characters for fossil types and extant species of *Nitraria*. There are no clear and consistent differences in the variability between fossil and extant taxa. Fossil taxa for which $N = 1$ were omitted from the analysis (Type 7, 18 and 29).

Figure S2. SEM micrographs of fossil *Nitraria* pollen, Plate 1. A 1-3, *Nitraripollis*/*Nitrariadites* sp. Age 37.28 Mya (3-37XJ_P2). Loose striae with perforations on the exine surface. B 1-3, *Nitraripollis*/*Nitrariadites* sp. Age 36.37 Mya (3_37XJ_P1). Wide striae with perforations on the exine surface. C 1-3, *Nitraripollis*/*Nitrariadites* sp. Age 36.37 Mya (3_37XJ_P1). Wide striae with perforations on the exine surface.
Figure S3. SEM micrographs of fossil and modern *Nitraria* pollen, Plate 2. A 1-2, *Nitraria retusa*. Note the perforations on the exine surface. Reproduced from Woutersen *et al.* (2018). B 1-2, *Nitraria sphaerocarpa*. 'Tight' striae on the exine surface. Reproduced from Woutersen *et al.* (2018). C 1-2, *Nitraripollis*/*Nitrariadites* sp., type 4? 'Tight' striae on the exine surface. Reproduced from Hoorn *et al.* (2012). D 1-2, *Nitraripollis*/*Nitrariadites* sp. Age 36.37 Mya (3_37XJ_P1). Striae on the exine surface. E 1-2, *Nitraripollis*/*Nitrariadites* sp. Age 36.37 Mya (3_37XJ_P1). Striae on the exine surface. F 1-2, *Nitraripollis*/*Nitrariadites* sp. Age 36.37 Mya (3_37XJ_P1). Polar view, loose striae with perforations on the exine surface. G 1-3, *Nitraripollis*/*Nitrariadites* sp. Age 37.28 Mya (3-37XJ_P2). Loose striae with perforations on the exine surface.
Figure S4. Phylomorphospace derived from post-ordination ancestral state estimation. The first two axes account for 31% of the variance in the data, and contain a similar signal to the pre-ordination ancestral state estimation phylomorphospace shown in Figure 5a, b.
Figure S5. Phylomorphospace generated using NMDS. A three-axis solution gave a stress value of 0.14. The distribution of taxa on the first two axes is highly similar to the phylomorphospace shown in Figure 5a, b.
Figure S6. Higher axes of the phylomorphospace shown in Figure 5a. (a) PCO axes 3 and 4; (b) 5 and 6.
Table S1. Previous records and identifications of *Nitraria* in the literature.